Acetylcholine production by group 2 innate lymphoid cells promotes mucosal immunity to helminths

Roberts, Luke B; Schnoeller, Corinna; Berkachy, Rita; Darby, Matthew; Pillaye, Jamie; Oudhoff, Menno J; Parmar, Naveen; Mackowiak, Claire; Sedda, Delphine; Quesniaux, Valerie; Ryffel, Bernhard; Vaux, Rachel; Gounaris, Kleoniki; Berrard, Sylvie; Withers, David R; Horsnell, William G C; Selkirk, Murray E

DOI:
10.1126/sciimmunol.abd0359

Title

Acetylcholine production by type 2 innate lymphoid cells promotes mucosal immunity to helminths

Authors

Luke B. Roberts[1,2], Corinna Schnoeller[1], Rita Berkachy[1], Matthew Darby[3], Jamie Pillaye[3,4], Menno J Oudhoff[5], Naveen Parmar[5], Claire Mackowiak[3], Delphine Sedda[6], Valerie Quesniaux[6], Bernhard Ryffel[6], Rachel Vaux[1], Kleoniki Gounaris[1], Sylvie Berrard[7], David R. Withers[4], William G. C. Horsnell[3,4,6,*], and Murray E. Selkirk[1,8,*]

Affiliations

[1]Department of Life Sciences, Imperial College London, London, UK.

[2]School of Immunology and Microbial Sciences, King's College London, Great Maze Pond, London SE1 9RT, UK.

[3]Wellcome Centre for Infectious Diseases Research in Africa, Institute of Infectious Disease and Molecular Medicine, University of Cape Town, Cape Town, South Africa.

[4]College of Medical and Dental Sciences, University of Birmingham, Birmingham, UK

[5]CEMIR – Centre of Molecular Inflammation Research, Department of Clinical and Molecular Medicine, NTNU – Norwegian University of Science and Technology, 7491 Trondheim, Norway

[6]Laboratory of Molecular and Experimental Immunology and Neurogenetics, UMR 7355, CNRS-University of Orleans and Le Studium Institute for Advanced Studies, Rue Dupanloup, 45000 Orléans, France.

[7] Université de Paris, NeuroDiderot, Inserm, 75019 Paris, France

[8]Further information and requests for resources and reagents should be directed to and will be fulfilled by the Lead Contact, Murray E. Selkirk (m.selkirk@imperial.ac.uk)

*Correspondence: ME Selkirk, m.selkirk@imperial.ac.uk; WGC Horsnell, wghorsnell@gmail.com

Abstract

Innate lymphoid cells (ILCs) are critical mediators of immunological and physiological responses at mucosal barrier sites. Whereas neurotransmitters can stimulate ILCs, the synthesis of small-molecule neurotransmitters by these cells has only recently been appreciated. Type 2 innate lymphoid cells (ILC2s) are shown here to synthesize and release acetylcholine (ACh) during parasitic nematode infection. The cholinergic phenotype of pulmonary ILC2s was associated with their activation state, could be induced by *in vivo* exposure to extracts of *Alternaria alternata* or the alarmin cytokines interleukin (IL)-33 and IL-25, and was augmented by IL-2 *in vitro*. Genetic disruption of ACh synthesis by murine ILC2s resulted in increased parasite burdens, lower numbers of ILC2s, and reduced lung and gut barrier responses to *Nippostrongylus brasiliensis* infection. These data demonstrate a functional role for ILC2-derived ACh in the expansion of ILC2s for maximal induction of type 2 immunity.

One-sentence summary

Synthesis of acetylcholine by type 2 innate lymphoid cells is important for optimal immune responses to helminth infection.

MAIN TEXT

Introduction

Acetylcholine (ACh) is best known as a small-molecule neurotransmitter, but its role in cholinergic signaling also regulates the immune system. This is best described in the cholinergic anti-inflammatory pathway (CAIP), in which sensory perception of inflammatory stimuli leads to a vagal reflex culminating in α7 nicotinic receptor (nAChR) subunit-dependent inhibition of TNF-α, IL-1β and IL-18 production by splenic macrophages (*1*, *2*) . The identification of cells that synthesize ACh has been facilitated by the use of reporter mice to visualize expression of choline acetyltransferase (ChAT), the enzyme which synthesizes ACh (*3*). $CD4^+$ T cells with an effector/memory ($CD44^+CD62L^{lo}$) phenotype were identified as the source of ACh in the spleen responsible for signaling to macrophages in the CAIP (*4*), and B cell-derived ACh inhibited neutrophil recruitment during sterile endotoxemia (*5*). Additionally, $CD4^+$ and $CD8^+$ T cell expression of

ChAT induced by IL-21 is essential for tissue trafficking required for T cell-mediated control of viral infection (*6*). Adaptive immunity is also regulated by ACh, and optimal type 2 effector responses to the nematode parasite *Nippostrongylus brasiliensis* require signaling through the M3 muscarinic receptor (mAChR) (*7*).

Group 2 innate lymphoid cells (ILC2s) play an important role in initiating type 2 immune responses, producing cytokines such as IL-13 and IL-5, which drive allergic inflammation and immunity to helminth infection (*8, 9*). ILC2s have been shown recently to be both positively and negatively regulated by neurotransmitters such as neuromedin U (NMU) (*10–12*) and noradrenaline (*13*) , whereas group 3 innate lymphoid cells (ILC3s) upregulate lipid mediator synthesis in response to vagally-derived ACh (*14*). Interestingly, ILCs expressing receptors responsive to neurotransmitters colocalize with neurons in mucosal tissues, forming neuroimmune cell units (NICUs) (*15*). ILC2s also express the neuropeptide calcitonin gene-related protein, CGRP (*16*). ILC2s have been shown to express tryptophan hydroxylase 1 (Tph1), which is the rate-limiting enzyme for the synthesis of the small-molecule neurotransmitter serotonin and have also been shown to produce serotonin (*17*).

In this study, we demonstrate that pulmonary ILC2s upregulate their capacity to synthesize and release ACh during infection with *N. brasiliensis*, and we show that the cholinergic phenotype of ILC2s is induced by the alarmin cytokines IL-33 and IL-25. *Ror*a^{Cre+}*Chat*^{LoxP} transgenic mice, which have ILC2s that do not synthesize ACh, have impaired immunity to *N. brasiliensis*, reduced expression of type 2 cytokines IL-5 and IL-13 in the lung, the mucins Muc5b and Muc5ac in the lung, and altered intestinal barrier responses. These data demonstrate that the production and release of ACh by ILC2s is an important factor in driving type 2 immunity.

Results

ILC2s synthesize and release acetylcholine during type 2 immunity

The cholinergic phenotype of immune cells was monitored across the time course of a primary infection with *N. brasiliensis* using ChAT-eGFP^{BAC} mice (*3*). From day 4 post infection (D4 p.i., immediately following the pulmonary migratory phase of parasite larvae) until at least D21 p.i., (long past the peak of the acute phase of infection-driven inflammation) the proportion and number of CD45^{+} cells in lung tissue that expressed ChAT (ChAT-eGFP^{+}) was elevated compared with uninfected (naïve) controls (**Figure 1A**). Analysis of ChAT-eGFP^{+} leukocytes revealed that most of these cells were from lymphoid rather than myeloid lineages, as previously reported in other models and tissues (*5*) (**Figure 1B**). Of the populations screened, expression of ChAT-eGFP was dramatically upregulated only in ILC2s at an early time point (D4) in infection (**Figure 1B, Figure S1A**).

ChAT-eGFP expression by ILC2s in lung and bronchoalveolar lavage (BAL) samples increased by D4 p.i., peaked at D7, and remained elevated in both sites at D21. The proportion of ILC2s that were ChAT-eGFP^{+} was consistently greater in BAL than in the lungs (**Figure 1C, 1D**). Real-time (RT)-qPCR confirmed that *Chat* expression in pulmonary ChAT-eGFP^{+} ILC2s from infected ChAT-eGFP^{BAC} mice was upregulated in comparison to ILC2 from uninfected ChAT-eGFP^{BAC} animals, as well as to ChAT-eGFP^{neg} ILC2, validating our reporter system (**Figure 1E**). HPLC-mass spectrometry was used to verify that WT ILC2s synthesize and release ACh and showed that this was greatly enhanced during parasite infection (**Figure 1F**). In these experiments, cells were isolated from infected animals at D11 p.i. to maximize the number of ACh-producing ILC2s obtained. We observed that ChAT-eGFP^{+} ILC2s had an increased mean fluorescence intensity (MFI) for the IL-33 receptor subunit ST2 compared with ChAT-eGFP^{-} cells at D4 and D7 p.i. (**Figure 1G**), and for inducible T cell co-stimulator (ICOS) at D7 p.i. (**Figure 1H**), suggesting that ChAT expression is associated with ILC2 activation state.

A striking degree of heterogeneity exists amongst ILC2s, including subtypes such as tissue-resident ‘natural’ ILC2s (nILC2s) and tissue-infiltrating ‘inflammatory’ ILC2s (iILC2s), which have been described and delineated on the basis of differential levels of phenotypic marker expression in the lung

(*18*). The functions of these subtypes have physiological relevance with regard to anti-helminth immune responses, such as pulmonary mucus production (*9*). To further characterize pulmonary ChAT-eGFP^{+} ILC2s and probe whether these cells belong to a defined subtype of ILC2s, we infected ChAT-eGFP^{BAC} mice with *N. brasiliensis* and analyzed pulmonary ILC2s at D7 p.i, utilizing an extended panel of phenotypic markers (**Figure 2A**). To assess whether ChAT-eGFP^{+} ILC2s represented previously recognized nILC2 and iILC2 subsets, we used t-distributed stochastic neighbor embedding (t-SNE) analysis (omitting ChAT-eGFP expression as a component for clustering), to first identify populations of ILC2s (CD45^{+}Lineage-CD127^{+}ICOS^{+} CD90^{+}cells expressing either or both ST2 and IL-17RB) that most resembled conventional nILC2 (IL-17RB^{-}ST2^{+}CD90^{+}Klrg1$^{lo/-}$) and iILC2 (IL-17RB^{+}ST2$^{lo/-}$ CD90^{lo} Klrg$^{+/hi}$) subsets (**Figure 2A**). We identified additional clusters that we designated 'nILCa' and 'iILC2a' as these populations appeared to represent nILC2-like and iILC2-like cells in a higher state of cellular activation, given their differential expression of IL-17RB, dual expression of ST2 and Klrg1, and higher expression of CD90. Given our previous observation that ChAT-eGFP expression in ILC2s appeared to correlate with cellular activation, we reasoned that these groupings may be relevant for comparative analysis. The majority of ILC2s expressing high levels of ChAT-eGFP were located among these activated nILC2a and iILC2a populations (**Figure 2B**). Analysis was again carried out utilizing t-SNE (with ChAT-eGFP expression incorporated into clustering), and ChAT-eGFP^{+} clusters could be segregated into 3 distinct populations, designated C1-C3 (**Figure 2C**). Based on a combination of marker expression and comparative assessment of the ChAT-eGFP^{+} clusters against the 4 pre-defined reference subtypes, population C1 appeared most similar to conventional nILC2 cells, whereas C2 shared the phenotypic profile of nILC2a, and C3 was most similar to iILC2a (**Figure 2D**). The greatest proportion of ChAT-eGFP^{+} ILC2s were represented by population C2, followed by C3, then C1 (**Figure 2E**). A similar analysis of marker expression of the very few ChAT-eGFP^{+} cells in naïve ChAT-eGFP^{BAC} lungs revealed that these cells clearly showed a nILC2-like profile, with no obvious differences in marker expression to that of total ChAT^{neg} ILC2s, including ICOS and ST2 (**Figure 2F, 2G, 2H**). A different scenario was observed in infected mice however, with a disparate profile for total ChAT-eGFP^{+} ILC2s relative to total ChAT^{neg} ILC2s (**Figure 2F, 2G, 2H**), corroborating the findings of previous

analyses (**Figure 1G, 1H**). ChAT-eGFP^{+} ILC2s do not therefore appear to represent a singular ILC2 subtype during *N. brasiliensis* infection.

We examined ILC2s from mesenteric lymph nodes (MLNs) to determine if ChAT-eGFP expression by ILC2s was a unique feature of pulmonary tissues. ChAT-eGFP^{+} ILC2 were found in MLNs of both naïve and *N. brasiliensis*-infected mice (**Figure 3A**). However, as in pulmonary populations, the proportion and total number of ILC2s expressing ChAT-eGFP increased during infection (**Figure 3B, 3C**). ChAT-eGFP^{+} ILC2s in the MLNs of infected mice displayed a different phenotypic profile to ChAT-eGFP^{neg} ILC2s, particularly based on Klrg1 expression, which was restricted to ChAT-eGFP^{+} cells, accompanied by higher expression of ST2, ICOS, and IL-17RB (**Figure 3D, 3E, 3F**). This difference in marker expression was also apparent between ChAT-eGFP^{+} and ChAT-eGFP^{neg} ILC2s of naïve MLNs, although expression levels were much greater following infection (**Figure 3E, 3F**). Given the difficulty in isolating viable leukocytes from the small intestinal lamina propria (siLP) of *N. brasiliensis* infected mice, we were not able to analyze ChAT-eGFP expression by flow cytometry from siLP ILC2 during infection. siLP ILC2s from naïve mice did not show any notable expression of ChAT-eGFP (**Figure 3G**), indicating that siLP ILC2s do not constitutively display a cholinergic phenotype in the absence of infection, akin to our observations in naïve lungs. Overall, these data indicate that ChAT-eGFP expression by ILC2s is not limited to pulmonary populations and support association of the cholinergic phenotype with cellular activation.

We evaluated if induction of the cholinergic phenotype in ILC2s was specific to parasite infection or a general feature of type 2 immunity. Mice exposed to extracts of *Alternaria alternata*, a fungal plant pathogen linked to exacerbation of asthma, develop rapid onset type 2-driven eosinophilic airway inflammation(*19*). ChAT-eGFP^{BAC} and WT mice were dosed intranasally with *Alternaria* extract or phosphate buffered saline (PBS), culled 24 hours later, and lung cells were analyzed for ChAT-eGFP expression. Successful induction of a type 2 response was confirmed by pulmonary eosinophilia (**Figure S1B**). Challenge with *Alternaria* induced a small increase in ChAT-eGFP expression in some lymphocyte populations, including CD4^{+} T cells and NKT cells, although expression in granulocytes

was unaffected (**Figure S1C**). As observed during nematode infection, the greatest proportional increase in ChAT-eGFP expression was observed in ILC2s (**Figures S1D, S1E**).

IL-25 and IL-33 induce the cholinergic phenotype of pulmonary ILC2s

Our data suggested that ChAT expression was associated with cellular activation, leading us to investigate whether known activators of ILC2s could induce this phenotype. Ex vivo stimulation of $CD45^+$ cells isolated from naïve $ChAT^{BAC}$-eGFP reporter mice with IL-33, but not IL-7, enhanced ILC2 ChAT-eGFP expression, suggesting that activation through alarmin signaling pathways specifically drives the ILC2 cholinergic phenotype (**Figure 4A**). To explore this further, we dosed reporter mice intranasally with IL-33, IL-25 and thymic stromal lymphopoietin (TSLP), and analyzed ChAT-eGFP expression on pulmonary ILC2s 24 h later. IL-25 and IL-33 both induced ChAT-eGFP expression on ILC2s, although no effect was observed with TSLP (**Figure 4B-C**). Analysis of other leukocyte populations in the lung showed that activation of ChAT-eGFP expression by alarmins was only observed in ILC2s at the time point investigated (**Figure 4D**).

Lung ILC2s predominantly express the IL-33 receptor in naïve animals at immunological baseline, whereas iILC2s expressing the IL-25 receptor are thought to migrate to the lung from sites such as the gut following tissue damage such as that caused by helminth infection (*18*). It is possible that administration of recombinant IL-25 mobilized ILC2s from outside the lungs to migrate to the pulmonary tract and that these cells contributed to the increase in ChAT-$eGFP^+$ ILC2s, although this is unlikely as it would have to happen within 24 h. Although the proportion of IL-17RB-expressing ILC2s in the lungs increased following *N. brasiliensis* infection (**Figure 4E, 4F**), approximately 20% of ILC2s from the lungs of naïve ChAT-$eGFP^{BAC}$ mice expressed IL-17RB as well as ST2 (**Figure 4E, 4F**), and thus have the capacity to respond to administration of exogenous IL-25.

To assess the capacity of lung-resident ILC2s to upregulate ChAT-eGFP, we isolated $CD45^+$ cells from the lungs of naïve $ChAT^{BAC}$-eGFP reporter mice and stimulated them *in vitro* with different

combinations of recombinant IL-33, IL-25, and IL-2, which are known to function as alarmins or promote proliferation and cytokine production (*20*, *21*). We assayed ChAT-eGFP expression by ILC2s after 24 h, and stimulation with IL-25 and IL-33 enhanced ChAT-eGFP expression. IL-2 also induced ChAT-eGFP expression, and an additive effect of stimulation with IL-2 and either IL-33 or IL-25 was observed (**Figure 4G-H**).

RoR*α*-driven disruption of ChAT expression impairs pulmonary type 2 immunity to *N. brasiliensis*

To determine whether synthesis of ACh by ILC2s played a role in immunity to helminth infection, we generated *Rora*$^{Cre+}$*Chat*^{LoxP} mice in which a portion of the coding domain of the *Chat* gene is floxed (*22*) and excised by Cre-recombinase expressed under the control of *Rora* regulatory elements (*23*) (**Figure S2A-B**). The use of *Rora*$^{Cre+}$ mice to selectively carry out gene deletion in ILC2s has been described previously (*24*). *Chat* deletion in *Rora*$^{Cre+}$*Chat*^{LoxP} ILC2s was confirmed by PCR analysis and sequencing (**Figure S2C, S2D, S2E).** Infection of *Rora*$^{Cre+}$*Chat*^{LoxP} and *Chat*^{LoxP} littermate controls with *N. brasiliensis* revealed that the number of larvae recovered from the lungs were not significantly different between genotypes at 2 dpi, but higher intestinal worm burdens were observed at day 6 p.i. in *Rora*$^{Cre+}$*Chat*^{LoxP} mice, indicating delayed parasite clearance in the absence of ILC2 ChAT expression (**Figure 5A**). *Rora*$^{Cre+}$*Chat*^{LoxP} mice had reduced pulmonary eosinophilia compared with controls following *N. brasiliensis* infection, indicative of a suppressed type 2 immune response (**Figure 5B**). Reduced expression of *Il5* and *Il13* in total lung tissue of infected *Rora*$^{Cre+}$*Chat*^{LoxP} samples, relative to controls supported this observation (**Figure 5C**). During the anti-helminth immune response, IL-13 drives goblet cell hyperplasia and mucin production at epithelial barrier sites including the lung, where the predominant gel-forming mucins secreted by goblet cells are Muc5b and Muc5ac (*25*). Infected *Rora*$^{Cre+}$*Chat*^{LoxP} at D6 p.i. demonstrated reduced expression of *Muc5b* and *Muc5ac* in total lung tissue (**Figure 5D**). PAS staining also revealed significantly reduced airway mucins in *Rora*$^{Cre+}$*Chat*^{LoxP} lungs compared with the robust response observed in *Chat*^{LoxP} airways (**Figure 5E-F**).

Impaired immunity to *N. brasiliensis* in *Rora*$^{Cre+}$*Chat*^{loxP} mice is associated with defective intestinal barrier responses

We assessed whether a defective response to *N. brasiliensis* infection following RoRα-mediated ChAT disruption was confined to pulmonary ILC2s and associated responses in the lung by evaluating responses in the small intestine. Intestinal epithelial effector responses characteristic of type 2 immunity include goblet and tuft cell hyperplasia. In the small intestine, we observed a decrease in periodic acid-Schiff (PAS)-positive goblet cells comparing *Rora*$^{Cre+}$*Chat*^{LoxP} samples to *Chat*^{LoxP} control samples (**Figure 6A, 6B).** We quantified tuft cells as analyzed through immunofluorescent staining of doublecortin-like kinase 1 (Dclk1) (**Figure 6C**) and observed that *Rora*$^{Cre+}$*Chat*^{LoxP} mice did not have a statistically reduced number of tuft cells overall (**Figure 6D**), but the ratio of cells present in villus versus crypt regions was lower in *Rora*$^{Cre+}$*Chat*^{LoxP} mice (**Figure 6E**). These data reflect a delayed and limited onset of type 2 immunity, which is in line with delayed worm expulsion (**Figure 5A)**.

ILC2-derived ACh promotes autocrine population expansion of ILC2s to facilitate optimal anti-helminth type 2 immunity.

ILC2s are the major innate source of IL-13 during helminth infection, and ILC2-derived IL-13 is critical for expulsion of *N. brasiliensis* and induction of mucin expression in response to helminth infections (*8, 9, 26*). We observed that RoRα-mediated disruption of *Chat* expression negatively impacted the type 2 immune response to *N. brasiliensis* infection, and we next analyzed whether ILC2s themselves were affected by removing their capacity to synthesize ACh. The total number of ILC2s in the lung increased following *N. brasiliensis* infection regardless of genotype, but fewer ILC2s were found in the lungs of *Rora*$^{Cre+}$*Chat*^{LoxP} mice (**Figure 7A**). Slightly fewer ILC2s were also observed in *Rora*$^{Cre+}$*Chat*^{LoxP} lungs compared with *Chat*^{LoxP} lungs at baseline (**Figure 7A**), and the fold change for infection-induced increases in ILC2 numbers at this timepoint was not significantly different between genotypes (**Figure S3A)**. A similar finding was made in the MLNs of infected *Rora*$^{Cre+}$*Chat*^{LoxP} mice, where fewer ILC2s were observed in comparison to infected controls (**Figure S3B**). Although ILC2s from *Rora*$^{Cre+}$*Chat*^{LoxP} mice could still express IL-5 and IL-13 (**Figure S3C-S3G**), the overall number of IL-13^{+} and IL-5^{+} ILC2s was significantly reduced in infected *Rora*$^{Cre+}$*Chat*^{LoxP} lungs at day 6 p.i. (**Figure 7B**).

Ki67 staining of ILC2s revealed that *Rora*$^{Cre+}$*Chat*^{LoxP} ILC2s proliferated less than *Chat*^{LoxP} ILC2s following infection (**Figure 7C, 7D**), resulting in a smaller pool of proliferative ILC2s overall (**Figure 7E**). Expression of ICOS was reduced on *Rora*$^{Cre+}$*Chat*^{LoxP} ILC2s following infection, indicative of a decreased ILC2 activation state (**Figure 7F, 7G**). Similar observations were made for the activation markers ST2 and ICOS on ILC2s in the MLNs of infected *Rora*$^{Cre+}$*Chat*^{LoxP} (**Figure S3H, S3I**), indicating that the effects caused by prevention of ACh synthesis were not confined to pulmonary ILC2s. We also analyzed the number of CD4^{+} lung T cells (**Figure S4A**), their proliferative capacity (**Figure S4B, S4C**), and expression of IL-13 (**Figure S4D**), but found that these parameters were unaffected by genotype, indicative of an ILC2-specific effect of *Chat* deletion in *Rora*$^{Cre+}$*Chat*^{LoxP} mice.

Lymphocytes are known to express acetylcholine receptors, although the full complement of muscarinic (mAChR) and nicotinic (nAChR) receptors expressed by ILC2s has not been defined to our knowledge (*7*, *27*). Using cDNA prepared from FACS-purified ChAT-eGFP^{+} and ChAT-eGFP^{neg} lung ILC2s from *N. brasiliensis*-infected ChAT-eGFP^{BAC} mice, we observed expression of transcripts for multiple mAChRs in addition to the α7nAChR (*27*). Interestingly, there appeared to be a degree of differential expression between ChAT-eGFP^{+} and ChAT-eGFP^{neg} with regards to AChR subtypes (**Figure 7H, 7I**). In order to determine whether ACh might act as an autocrine factor to influence proliferation and activation of the cells, we isolated WT ILC2s from the lungs of *N. brasiliensis*-infected C57BL/6J mice and cultured them in vitro with IL-7 and IL-2 alone or in the presence of the mAChR antagonist 1,1-dimethyl-4-diphenylacetoxypiperidinium iodide (4-DAMP) or the nAChR antagonist mecamylamine. Addition of 4-DAMP restricted the proliferative capacity of the cells, whereas mecamylamine had no effect when compared with vehicle-treated control cultures (**Figure 7J, 7K, 7L**). These data suggest that activation-induced ACh synthesis by ILC2s plays a role in mAChR-mediated autocrine promotion of ILC2 proliferation and population expansion.

Discussion

ILC2s play a pivotal role in translating epithelial cell cytokine production into robust type 2 immune responses. Here we show that in addition to the cytokines IL-13 and IL-5, production of ACh by ILC2s is a requirement for optimal type 2-driven immunity to *N. brasiliensis*. The alarmin cytokines IL-25 and IL-33 upregulated ChAT-eGFP expression by ILC2s both in vivo and in vitro. As expression of ChAT by B cells is induced by MyD88-dependent Toll-like receptor signaling (*5*), we hypothesised that IL-33 might regulate the ILC2 cholinergic phenotype, as members of the IL-1 family such as IL-33 also signal through this adapter protein. IL-25 was also a major regulator of ChAT expression, demonstrating that MyD88-dependent signaling is not essential for this in ILC2s. A factor common to both signaling pathways, such as the signal transducer TRAF6, may be required for inducible ChAT expression in ILC2s. TSLP, which does not signal through either MyD88 or TRAF6-dependent pathways, did not induce ChAT expression in ILC2s when administered in vivo at the same dose. TSLP has been reported to influence cutaneous ILC2 activation (*28*), but most studies identify IL-25 and IL-33 as the major inducers of ILC2 responses in the lung and gut (*26*, *29*).

IL-2 was also shown to induce ChAT expression by itself or in combination with IL-25 and IL-33. IL-2 is a critical regulator of ILC2s, driving cell survival and proliferation and augmenting type 2 cytokine production (*30*). The cholinergic phenotype of ILC2s can be induced by a number of stimuli that activate these cells. Recently, neuropeptides such as NMU, vasoactive intestinal peptide (VIP) and CGRP and the small molecule neurotransmitter serotonin have also been shown to regulate ILC2 activation and effector activity (*10–12*, *16*, *17*, *31*). If these molecules can also induce or modulate ChAT expression in ILC2s, this raises the possibility of bidirectional neuroimmune communication involving ILC2s and ACh-responsive neurons within NICUs.

Impairment of ACh synthesis by ILC2s resulted in a lower number of cells, a deficit in ILC2-derived effector cytokine production, and striking restriction of anti-helminth type 2 responses in the lungs and small intestine, tissue sites physiologically relevant to the parasite's life cycle. Lower numbers of ILC2s in the lungs and MLN of uninfected *Rora*$^{Cre+}$*Chat*^{LoxP} mice is suggestive of a homeostatic requirement for ACh, and one interpretation of this may be that ILC2-derived ACh acts as an autocrine signal to aid

population expansion. ACh may promote expression of autocrine survival factors such as IL-9 (*32*), the expression of which has been shown to be promoted by neuropeptide signaling in ILC2s (*33*). The labile nature of ACh, due to high levels of circulating butyrylcholinesterase in tissue fluids (*34*) makes it likely that ILC2-derived ACh will function over relatively short distances, as would be the case during autocrine signaling. In support of this, we demonstrated that ILC2s express a range of nicotinic and muscarinic ACh receptors, and expression of the α7 nAChR by ILC2s has also been previously described (*27*). In vitro culture of ILC2s with 4-DAMP led to a reduction in ILC2 proliferative capacity. Thus it is plausible that autocrine cholinergic signaling in ILC2s operates through mAChRs in order to promote their own expansion. Although 4-DAMP is frequently quoted as M3/M1-selective, studies on rat and human receptors show that it has potent effects on M1, M3, M4 and M5 receptors (K_i less than 1 nM), and also good activity against M2 (K_i 4-7 nM). (*35*, *36*). Thus, at the concentration used in our experiments, 4-DAMP would be expected to antagonise all mAChR subtypes.

Anticholinergics in the form of mAChR antagonists such as tiotropium are widely used to treat asthma and chronic obstructive pulmonary disease (*37*). These antagonists alleviate bronchoconstriction and mucus production, and are well documented to ameliorate allergen-induced airway inflammation and remodeling (*38*, *39*), which may be accompanied by reduced type 2 cytokine production (*40*). In contrast, a recent report indicated that an α7-selective nAChR agonist reduced ILC2 effector function and airway hyperreactivity in an *Alternaria* allergic inflammation model (*27*). It is likely that signaling through different AChRs on ILC2s can result in disparate outcomes, and this could be affected by altered receptor expression under differing physiological conditions.

A surprising observation was that ChAT expression by ILC2s was maintained several weeks after helminth eradication from the host (D21 p.i.). In addition to critical type 2 effector functions, ILC2s play important direct and indirect roles in promotion of wound healing and tissue repair (*41*, *42*). It will be interesting to determine whether ACh production by ILC2s plays a role during later, pro-repair activities in addition to the acute inflammatory phase of infection.

A limitation of our study is that, despite the critical role of RoRα in ILC2 development (*43, 44*), expression of RoRα is not confined to ILC2s (*45*). Therefore, despite the fact that the *Rora*$^{Cre+}$ mouse has previously been used to successfully facilitate gene deletion in ILC2s in vivo (*24*), it is feasible that deletion in other cell types may also have occurred, and that this may have contributed to our observations. However, proliferation and Th_2 cytokine production by $CD4^+$ T cells, which are also known to express this transcription factor, were not affected during *N. brasiliensis* infection of *Rora*$^{Cre+}$*Chat*^{LoxP} mice.

Helminths have evolved sophisticated strategies to promote survival in their hosts, targeted at key drivers of anti-parasite immunity (*46*). Secretion of acetylcholinesterases (AChEs) by parasitic nematodes has been postulated to promote parasite persistence via inhibition of cholinergic signaling in relation to the 'weep and sweep' response, characterized by intestinal smooth muscle contraction and fluid secretion from epithelial cells (*47*). Our current study demonstrates that production of ACh by ILC2s is a key factor in population expansion, driving maximal type 2 immunity and mucin expression, suggesting that hydrolysis of ACh by secreted AChEs may also act to suppress this to a level that allows for parasite establishment within the host.

Materials and Methods

Study design. The aim of this study was to determine the role of cholinergic signalling in the immune response to infection with a helminth parasite. We utilised ChAT-eGFP^{BAC} reporter mice and flow cytometry to determine which cells synthesized acetylcholine (ACh), and conducted a kinetic analysis on their cholinergic phenotype throughout infection with the nematode parasite *Nippostrongylus brasiliensis*. Real-time qPCR was used to verify alterations in expression of *Chat*, and mass spectrometry used to confirm cellular secretion of ACh. Induction of a cholinergic phenotype in another setting characteristic of type 2 immmunity was examined by intranasal administration of *Alternaria alternata* extracts and alarmin cytokines. The influence of ACh synthesis by ILC2s was investigated by generation of *Rora*$^{Cre+}$*Chat*^{LoxP} transgenic mice, and the effect on immunity to parasite infection

determined in comparison to *Chat*^{LoxP} littermate controls. Flow cytometry, cytokine ELISA, qPCR and histochemistry were used to characterise lung and gut barrier responses to parasite infection. Age and sex-matched mice were used for in vivo experiments, with group sizes between 3-6, conducted in replicates as indicated in figure legends. For flow cytometry experiments, negative controls were included to establish reliable gates for each marker. Parasite recoveries and histological scores were conducted in blinded conditions. No outliers were removed.

Animals and parasite infection. This study was approved by the Animal Welfare Ethical Review Board at Imperial College London and was licensed by and performed under the UK Home Office Animals (Scientific Procedures) Act Personal Project Licence number 70/8193: 'Immunomodulation by helminth parasites'. C57BL/6J mice, aged 6-8 weeks old were purchased from Charles River. ChAT-eGFP^{BAC} (*3*) were purchased from Jackson Laboratories and subsequently bred in-house. *Chat*^{LoxP} mice were generated as previously described (*22*) and were backcrossed to F6-F10 generations on a B6 background with *Rora*$^{Cre+}$ (*23*) a kind gift from Andreas Zembrzycki (Salk Institute, La Jolla, CA) to generate the *Rora*$^{Cre+}$*Chat*^{Loxp} mice used in this study. Mice were infected with *N. brasiliensis* by sub-cutaneous (s.c.) inoculation with 500 infective larvae and parasites maintained by established methods (*48*).

Murine model of allergic airway inflammation. Extracts of *Alternaria alternata* were obtained as a gift from Henry McSorley (University of Edinburgh) or purchased as lyophilized protein extract from Greer Laboratories (USA). Mice were lightly dosed with isoflurane before intranasal administration with 50 µg *A. alternata* extract in a final volume of 50 µl PBS. Mice were exposed to a single dose of *A. alternata* for 24 hours. Control animals were dosed with 50 µl PBS following the same schedule.

Cytokines. Recombinant murine cytokines were purchased from R&D (IL-25, TSLP) or Peprotech (IL-33, IL-2, IL-7) and used at 50 ng ml^{-1} *in vitro* or administered in 50 µl doses at 10 µg ml^{-1} *in vivo* as indicated.

Tissue preparation. For isolation of bronchoalveolar cells, lungs were lavaged twice in a total of 2 ml PBS with 0.2% BSA and 2 mM EDTA. Erythrocytes were lysed, leukocytes resuspended and counted. For lung single cell suspensions, lungs were perfused via cardiac puncture with 10 ml PBS then infused with 1.5 ml PBS containing 5 mg ml^{-1} dispase II neutral protease (Sigma) via the trachea. The thymus and lung-draining lymph nodes were removed, lungs ligatured, removed into 1.5 ml digest solution, incubated at room temperature for 25 min, then for a further 30 min at 37ºC. Lungs were mechanically dissociated in Dulbecco's Minimal Essential Medium (DMEM) with 25 mM HEPES and 100 U ml^{-1} DNAse I (Sigma), and incubated at room temperature for 10 min. Samples were passed through 100 μm cell strainers and erythrocytes lysed.

Single cell preparations of mesenteric lymph nodes were generated by mechanical dissociation through a 40 μm cell strainer followed by standard erythrocyte lysis. Small intestinal lamina propria (siLP) leukocytes were isolated with EDTA-based stripping of the intestinal epithelial layer followed by tissue digestion using collagenase-D (0.5 mg ml^{-1}), Dispase-II (1.5 mg ml^{-1}) and 10 μg ml^{-1} DNAse I in HBSS without Mg^{2+} or Ca^{2+} + 2% FCS. A 40-80% Percoll gradient separation was used to isolate a leukocyte enriched siLP sample.

Flow cytometry and cell sorting. Single cell suspensions were stained with fixable viability dyes (Invitrogen), then treated with rat anti-mouse CD32/CD16 (FcBlock, BD Biosciences), washed, then stained for extracellular markers using fluorophore conjugated monoclonal antibodies (eBioscience, Miltenyi Biotec or Biolegend). For intracellular staining, cells were fixed for 30 min at room temperature, then permeabilized using the FoxP3/transcription factor staining buffer kit (eBioscience) and stained with fluorochrome-conjugated antibodies. Unstained samples and fluorescence minus one controls were used as appropriate. When analyzing eGFP fluorescence from ChAT-eGFP^{BAC} reporter mouse cells, WT (C57BL/6J) cells were used as negative controls to set eGFP gates. Samples were analyzed on a BD LSR Fortessa™ analyzer. For FACS sorting of ILC2s, lung tissue was processed to a single cell suspension as described, the lineage negative population enriched by magnetic activated cell

sorting, depleting other cells via a PE-conjugated lineage cocktail (Miltenyi Biotec), then ILC2s sorted on a BD FACS ARIA III cell sorter.

Immunophenotyping of leukocyte populations. Unless otherwise stated, leukocyte populations were identified by flow cytometry by gating live cells, followed by single cell and $CD45^+$ gating, and then using the following markers: ILC2; $lineage^-CD90^+ICOS^+ST2^+CD127^+$. T cells; $CD19^-CD3\varepsilon^+$. $CD4^+$ T cells; $CD19^-CD3\varepsilon^+DX5^-CD4^+CD8\alpha^-$. $CD8^+$ T cells; $CD19^-CD3\varepsilon^+DX5^-CD4^-CD8\alpha^+$. B cells; $CD19^+CD3\varepsilon^-B220^+$. γδ T cells; $CD19^-CD3\varepsilon^+DX5^-CD4^-CD8\alpha^-GL3^+$. NK-T cells (NKT); $CD19^-CD3\varepsilon^+DX5^+$. Natural Killer cells (NK); $CD19^-CD3\varepsilon^-DX5^+FcεR1^-$. Neutrophils; $CD11b^+$SIGLEC-F^-GR-$1^{hi}CD11c^{lo}$ Eosinophils; $CD11b^+$SIGLEC-F^+GR-1^{lo} $CD11c^{lo}$. Basophils; $CD19^-CD3\varepsilon^-DX5^+FcεR1^+$. The lineage panel consisted of antibodies to CD3, CD4, CD8, B220, CD19, TER119, CD49b, FcεRI and CD11b. Additional markers analyzed for phenotyping and functional analysis were assessed using antibodies against Klrg1, IL-17RB, IL-5 and IL-13.

Ki67 and intracellular cytokine staining. To assess proliferative capacity of cells directly ex vivo, samples were processed to single cell suspension as described and rested in cDMEM (DMEM + 10% FCS, + 2mM L-glutamine + 100U ml^{-1} Penicillin + 100ug ml^{-1} streptomycin) for 1 hour at 37ºC/5%CO2, before extracellular staining, fixing and permeabilization as detailed. Intracellular Fc receptor blocking followed by anti-Ki67 staining was then carried out with fluorophore conjugated mAbs in permeabilization buffer. To assess cytokine production, single cell suspensions were diluted to 5x 10^6 cells ml^{-1} in cDMEM and either stimulated for 4 h at 37ºC/5% CO2 with 1 ug ml^{-1} PMA/100 ng ml^{-1} ionomycin with 1x Brefeldin-A (GolgiPlug, BD Biosciences) + 1μM Monensin ((Sigma) or left unstimulated (golgi -inhibitors alone). Samples were stained, fixed and permeabilized as described and intracellular staining for Fc receptor blocking followed by fluorophore conjugated mAbs against IL-5 and IL-13 was carried out in permeabilization buffer.

ILC2 in vitro culture and proliferation analysis with acetylcholine receptor antagonists. Female C57BL/6J mice aged 6-8 weeks were infected with *N. brasiliensis* and lungs were processed and ILC2

FACS sorted at between D5 to D9 p.i. as described. For each experimental run, lungs from 5 mice were pooled and sorted as a single sample and isolated ILC2 were then split equally between experimental treatment conditions. Cells were cultured for 72 hours at 37°C / 5% CO2 in U bottom 96 well plates (Greiner, Cellstar) in 200 µl of cRPMI (RPMI + 10% FCS + 2 mM L-glutamine + 100 U ml^{-1} Penicillin + 100 ug ml^{-1} streptomycin) containing 50 ng ml^{-1} recombinant human IL-2 (Biolegend) and 50 ng ml^{-1} recombinant murine IL-7 (Biolegend) and either 10 µM 1,1-dimethyl-4-diphenylacetoxypiperidinium iodide (4-DAMP) (Abcam), 10 µM mecamylamine hydrochloride (mecamylamine) (Sigma), or an equal volume of drug vehicle (dH20 and DMSO) (vehicle control). Finally, cells were stained as described, including re-staining using the extracellular ILC2 marker panel used to initially sort the cells (to ensure purity of the cultured population), followed by intranuclear Ki67 staining. Samples were analyzed on a BD LSR Fortessa™ analyzer.

Endpoint PCR. Total RNA was extracted by TRIzol/chloroform phase-separation and DNAse-1 treatment. Prior to RNA extraction, mouse brain tissue (used as a for positive control for all acetylcholine receptor subunit expressions) was homogenized using a Tissuelyser II (Qiagen). Reverse transcription (RT) of RNA was carried out in a 20 µl reaction volume with 50 ng RNA using the Superscript III reverse transcriptase protocol (Invitrogen) according to the manufacturer's instructions. Polymerase chain reaction (PCR) was carried out in a 20 µl reaction volume containing: 0.25 pmol forward and reverse primers, 1.25 mM dNTPs, 0.5 U Taq polymerase (New England Biolabs), 1x Thermopol reaction buffer (New England Biolabs), 2 µl cDNA and dH20. PCR products were visualized by agarose gel electrophoresis on a gel of appropriate agarose percentage (1-3%) made with a standard Tris-acetate-EDTA buffer (pH 8.0), utilising GelRed ® nucleic acid gel stain (Biotium) and a GelDOC-IT TS imaging system (UVP). Primers used for endpoint PCR are as follows:

Chrm1: 5'- GGACAACAACACCAGAGGAGA-3'/5'-CGAGGTCACTTTAGGGTAGGG-3'

Chrm2: 5'- TGAAAACACGGTTTCCACTTC-3'/5'- GATGGAGGAGGCTTCTTTTTG-3'

Chrm3: 5'- TTTACATGCCTGTCACCATCA-3'/5'- ACAGCCACCATACTTCCTCCT-3'

Chrm4: 5'- TGCCTCTGTCATGAACCTTCT-3'/5'- TGGTTATCAGGCACTGTCCTC-3'

Chrm5: 5'- CTCTGCTGGCAGTACTTGGTC-3'/5'-GTGAGCCGGTTTTCTCTTCTT-3'

Chrna1: 5’- GACCATGAAGTCAGACCAGGA-3’/5’- TTAGCTCAGCCTCTGCTCATC-3’

Chrna2: 5’- TGAGGTCTGAGGATGCTGACT-3’/5’- AGAGATGGCTCCAGTCACAGA-3’

Chrna3: 5’- GTTGTCCCTGTCTGCTCTGTC-3’/5’- CCATCAAGGGTTGCAGAAATA-3’

Chrna4: 5’- AGATGATGACGACCAACGTGT-3’/5’- ATAGAACAGGTGGGCTTTGGT-3’

Chrna5: 5’- TGGGCCTTGCAATATCTCAGT-3’/5’- TGACAGTGCCATTGTACCTGA-3’

Chrna7: 5’- TCAGCAGCTATATCCCCAATG-3’/5’- CAGCAAGAATACCAGCAAAGC-3’

Chrnb1: 5’- CTCACTGTGTTCTTGCTGCTG-3’/5’- GAGTTGGTCTCTCTCGGGTTT-3’

Chrnb2: 5’- GGACCATATGCGAAGTGAAGA-3’/5’- ATTTCCAGGGAAAAAGAAGCA-3’

Chrnb4: 5’- TGGCTGCCTGACATAGTTCTC-3’/5’- AGTCCAGGATCCGAACTTCAT-3’

RT-qPCR. Total lung tissue was homogenized using a Tissuelyser II (Qiagen). FACS purified cells were lysed directly in TRIzol (Sigma). Total RNA was extracted by TRIzol/chloroform phase-separation, DNAse-1 treated, then reverse transcribed using the iScript cDNA synthesis kit (Biorad). RT-qPCR reactions were carried out using either the PowerUp SYBR Green Mix (ThermoFisher) (*Il13, Il5, Muc5ac, Muc5b, Gapdh, Actb, Hprt*) or the Quantitect SYBR Green PCR kit (Qiagen) *(Chat, 18s*) in a ABI 7500 Fast Real-time PCR thermocycler (Applied Biosystems). RT-qPCR reactions were run in triplicate, with no template and no RT controls. Relative expression of each gene was calculated by the comparative cycle threshold (Ct) method ($2^{-\Delta\Delta CT}$) using *Actb, Hprt* and *Gapdh* (*Il13, Il5, Muc5ac,* Muc5b) and *18s* (*Chat*) as reference genes. Primer sequences used for RT-qPCR were as follows:

Chat; 5’-GGCCATTGTGAAGCGGTTTG-3’/5’-GCCAGGCGGTTGTTTAGATACA-3’,

18s; 5’-TAACGAACGAGACTCTGGCAT-3’/CGGACATCTAAGGGCATCACAG-3’.

Il13; 5’-TCACTGTAGCCTCCAGGTCTC-3’/5’-TTTCATGGCTGAGGGCTGGTT-3’.

Il5; 5’-AGCTGGATTTTGGAAAAGAAAAGGG-3’/5’-GCTTTCTGTTGGCATGGGGT-3’.

Muc5ac; 5’-GACACAAGCCATGCAGAGTCC-3’/5’-CTGGAAAGGCCCAAGCATGT-3’.

Muc5b; 5’-AGCATCAAAGAGGGTGGTGGG-3’/5’-CTTGCTGTGGGGAGCCTTAAC-3’.

Gapdh; 5’-GTCATCCCAGAGCTGAACGG-3’/5’-TACTTGGCAGGTTTCTCCAGG-3’.

Actb; 5’-TTCCTTCTTGGGTATGGAATCCT-3’/5’-TTTACGGATGTCAACGTCACAC-3’.

Hprt; 5’-ACAGGCCAGACTTTGTTGGA-3’/5’-ACTTGCGCTCATCTTAGGCT-3’

Genotyping. Genomic DNA (gDNA) was isolated from FACS-purified lung ILC2 from *Rora*$^{Cre+}$*Chat*^{LoxP} and WT mice at day 6 p.i. with *N. brasiliensis* using a DNeasy Blood and Tissue kit (Qiagen). PCR was performed with gDNA template using Q5 DNA polymerase (NEB) and the primers 5'-TGAGGGATGATGGATGAATGAG-3'/5'- CTAGGGTTGTTTCCAGAAGGC-3', situated within intronic regions flanking coding exon 5 of murine *Chat*. Amplified products were separated by agarose gel electrophoresis, and bands corresponding to the WT allele (2076 bp) and the deleted allele (546 bp) were excised, purified by standard procedures, and sequenced by Eurofins Genomics.

Detection of acetylcholine release. FACS-purified ILC2s were incubated at 37ºC for 30 min in 96 well round-bottomed plates (10^5 cells in 150 µl), centrifuged, supernatants removed, the AChE inhibitor BW284C51 (Sigma) added at 10 µM and samples stored at -80ºC until analysis by HPLC-mass spectrometry. Control samples were spiked with 50 nM internal standard (acetylcholine -1,1,2,2,-D4 chloride, QMX laboratories).

Histology and PAS staining. Lung or small intestinal tissues were harvested, fixed in 10% buffered formalin, paraffin embedded and sectioned using standard techniques. Sections were stained with periodic acid-Schiff's and Haematoxylin and Eosin reagents, photographed at 40x or 100x magnification using a Zeiss Primo Star microscope and analyzed using Image J to determine the Histological Mucus Index (HMI) by established methods (*49*). Lung sections were analyzed using ImageJ. Briefly, lung images were overlaid with a standard grid (2000 Units) and the number of grid units containing PAS positive epithelial cells were divided by all units containing epithelial cells to establish the Histological Mucus index (HMI). Intestinal images were analyzed with ImageJ and overlaid with a standard grid (1500 Units); 15 crypt-villus segments were selected and the percentage of PAS-positive units per crypt-villus segment were divided by total units in each crypt-villus to establish HMI.

Immunofluorescence. Jejunal sections were paraffin embedded and sectioned according to standard techniques. For immunofluorescent staining, tissue slides were incubated at 60°C for 30 min. Next, paraffin was removed in Neo-clear (Sigma-Aldrich) by washing twice for 5 min. Then, tissue was rehydrated in decreasing ethanol concentrations (2x 100%, 1x 95%, 1x 80 %, 1x 70 %, (all 3 min) and then in distilled water. Subsequently, tissue slides were heated and boiled in pH 6 citrate buffer for 15 min using a microwave. The citrate buffer was cooled to room temperature for 20 min, and slides were washed with distilled water. Next, tissues sections were marked using a hydrophobic pen (PAP pen, ab2601, Abcam) to prevent leakage. Tissue sections were incubated with blocking buffer (1% BSA, 2% normal goat serum, 0.2% Triton X-100 in PBS) for 1 hour at room temperature in a humified chamber. Next, slides were incubated with primary antibody for anti-DCLK1 (Abcam, ab31704) in antibody dilution buffer at 1:250 (0.5% bovine serum albumin, 1% normal goat serum, 0.05% Tween 20 in PBS) at 4°C overnight in a humified chamber. The next day, slides were washed 3 times in 0.2% Triton X-100 prepared in PBS for 10 min each. Slides were then incubated with the secondary antibody (1:500, Goat anti-Rabbit IgG Alexa Fluor 488, Invitrogen, A-11034,) and DAPI (1:1000) for 1 hour at room temperature in a dark humified chamber. After incubation, slides were washed 3 times with 0.2% Triton X-100 prepared in PBS for 10 min each. Finally, slides were washed with distilled water and were mounted using Fluoromount G medium (ThermoFisher Scientific) using cover slips. All the images were acquired with 20x and 40x objectives using a ZEISS confocal microscope LSM 880 and DCLK1 (green) cells were quantified for ≥30 crypt-villus pairs per mouse.

Statistical analysis. Flow cytometry data was analyzed and t-SNE analysis was conducted using FlowJo software (Treestar). Graphs and statistical tests were carried out using GraphPad Prism software (GraphPad). Normality of data distribution was analyzed by Shapiro-Wilk test. Parametric data were analyzed by Welch's t-test, non-parametric data were analyzed by Mann-Whitney-U test. Data represent mean ± SEM unless otherwise stated. Statistical significance between groups is indicated as *p<0.05, **p<0.01, ***p<0.001, ****p<0.0001, n.s. = non-significant difference (p>0.05).

H2: Supplementary Materials

Figure S1. Pulmonary ILC2s acquire a cholinergic phenotype following exposure to *Alternaria alternata*

Figure S2. Generation of *Rora*$^{Cre+}$*Chat*^{loxP} and validation of *Chat* deletion in lung ILC2s.

Figure S3. Pulmonary ILC2 cytokine measurements and assessment of numbers and activation markers of mesenteric lymph node ILC2s in *Chat*^{LoxP} and *Rora*$^{Cre+}$*Chat*^{LoxP} mice**.**

Figure S4. Pulmonary $CD4^+$ T cell numbers and capacity for Th_2 cytokine expression remains intact in *Rora*$^{Cre+}$*Chat*^{loxp} mice

Figure S5. Material Transfer Agreement with INEM/CNRS.

References and Notes

1. K. J. Tracey, The inflammatory reflex. *Nature*. **420**, 853–859 (2002).
2. H. Wang, M. Yu, M. Ochani, C. A. Amella, M. Tanovic, S. Susarla, J. H. Li, H. Wang, H. Yang, L. Ulloa, Y. Al-Abed, C. J. Czura, K. J. Tracey, Nicotinic acetylcholine receptor alpha7 subunit is an essential regulator of inflammation. *Nature*. **421**, 384–388 (2003).
3. Y. N. Tallini, B. Shui, K. S. Greene, K. Y. Deng, R. Doran, P. J. Fisher, W. Zipfel, M. I. Kotlikoff, BAC transgenic mice express enhanced green fluorescent protein in central and peripheral cholinergic neurons. *Physiol. Genomics*. **27**, 391–397 (2006).
4. M. Rosas-Ballina, P. S. Olofsson, M. Ochani, Y. A. L. Sergio I. Valdés- Ferrer, C. Reardon, M. W. Tusche, V. A. Pavlov, U. Andersson, S. Chavan, T. W. Mak, and K. J. Tracey, Acetylcholine-Synthesizing T Cells Relay Neural Signals in a Vagus Nerve Circuit. *Science.* **334**, 98–101 (2015).
5. C. Reardon, G. S. Duncan, A. Brüstle, D. Brenner, M. W. Tusche, P. Olofsson, M. Rosas-Ballina, K. J. Tracey, T. W. Mak, Lymphocyte-derived ACh regulates local innate but not adaptive immunity. *Proc. Natl. Acad. Sci. U. S. A.* **110**, 1410–1415 (2013).
6. M. A. Cox, G. S. Duncan, G. H. Y. Lin, B. E. Steinberg, L. X. Yu, D. Brenner, L. N. Buckler, A. J. Elia, A. C. Wakeham, B. Nieman, C. Dominguez-Brauer, A. R. Elford, K. T. Gill, S. P. Kubli, J. Haight, T. Berger, P. S. Ohashi, K. J. Tracey, P. S. Olofsson, T. W. Mak, Choline acetyltransferase–expressing T cells are required to control chronic viral infection. *Science.*

363, 639–644 (2019).

7. M. Darby, C. Schnoeller, A. Vira, F. Culley, S. Bobat, M. E. Selkirk, W. G. C. Horsnell, The M3 Muscarinic Receptor Is Required for Optimal Adaptive Immunity to Helminth and Bacterial Infection, *PLoS Pathog.* 11, e1004636 (2015).

8. D. R. Neill, S. H. Wong, A. Bellosi, R. J. Flynn, M. Daly, T. K. a Langford, C. Bucks, C. M. Kane, P. G. Fallon, R. Pannell, H. E. Jolin, A. N. J. McKenzie, Nuocytes represent a new innate effector leukocyte that mediates type-2 immunity. *Nature*. **464**, 1367–70 (2010).

9. L. Campbell, M. R. Hepworth, J. Whittingham-Dowd, S. Thompson, A. J. Bancroft, K. S. Hayes, T. N. Shaw, B. F. Dickey, A. L. Flamar, D. Artis, D. A. Schwartz, C. M. Evans, I. S. Roberts, D. J. Thornton, R. K. Grencis, ILC2s mediate systemic innate protection by priming mucus production at distal mucosal sites. *J. Exp. Med.* **216**, 2714–2723 (2019).

10. V. Cardoso, J. Chesné, H. Ribeiro, B. Garcia-Cassani, T. Carvalho, T. Bouchery, K. Shah, N. L. Barbosa-Morais, N. Harris, H. Veiga-Fernandes, Neuronal regulation of type 2 innate lymphoid cells via neuromedin U. *Nature*. **549**, 277–281 (2017).

11. C. S. N. Klose, T. Mahlakõiv, J. B. Moeller, L. C. Rankin, A.-L. Flamar, H. Kabata, L. A. Monticelli, S. Moriyama, G. G. Putzel, N. Rakhilin, X. Shen, E. Kostenis, G. M. König, T. Senda, D. Carpenter, D. L. Farber, D. Artis, The neuropeptide neuromedin U stimulates innate lymphoid cells and type 2 inflammation. *Nature*. **549**, 282–286 (2017).

12. A. Wallrapp, S. J. Riesenfeld, P. R. Burkett, R. E. E. Abdulnour, J. Nyman, D. Dionne, M. Hofree, M. S. Cuoco, C. Rodman, D. Farouq, B. J. Haas, T. L. Tickle, J. J. Trombetta, P. Baral, C. S. N. Klose, T. Mahlakõiv, D. Artis, O. Rozenblatt-Rosen, I. M. Chiu, B. D. Levy, M. S. Kowalczyk, A. Regev, V. K. Kuchroo, The neuropeptide NMU amplifies ILC2-driven allergic lung inflammation. *Nature*. **549**, 351–356 (2017).

13. S. Moriyama, J. R. Brestoff, A. L. Flamar, J. B. Moeller, C. S. N. Klose, L. C. Rankin, N. A. Yudanin, L. A. Monticelli, G. G. Putzel, H. R. Rodewald, D. Artis, β2-Adrenergic Receptor-Mediated Negative Regulation of Group 2 Innate Lymphoid Cell Responses. *Science.* **359**, 1056–1061 (2018).

14. J. Dalli, R. A. Colas, H. Arnardottir, C. N. Serhan, Vagal Regulation of Group 3 Innate

Lymphoid Cells and the Immunoresolvent PCTR1 Controls Infection Resolution. *Immunity*. **46**, 92–105 (2017).

15. H. Veiga-Fernandes, D. Artis, Neuronal-immune system cross-talk in homeostasis. *Science.* **359**, 1465–1466 (2018).

16. H. Nagashima, T. Mahlakõiv, H. Y. Shih, F. P. Davis, F. Meylan, Y. Huang, O. J. Harrison, C. Yao, Y. Mikami, J. F. Urban, K. M. Caron, Y. Belkaid, Y. Kanno, D. Artis, J. J. O'Shea, Neuropeptide CGRP Limits Group 2 Innate Lymphoid Cell Responses and Constrains Type 2 Inflammation. *Immunity*. **51**, 682-695 (2019).

17. A. L. Flamar, C. S. N. Klose, J. B. Moeller, T. Mahlakõiv, N. J. Bessman, W. Zhang, S. Moriyama, V. Stokic-Trtica, L. C. Rankin, G. G. Putzel, H. R. Rodewald, Z. He, L. Chen, S. A. Lira, G. Karsenty, D. Artis, Interleukin-33 Induces the Enzyme Tryptophan Hydroxylase 1 to Promote Inflammatory Group 2 Innate Lymphoid Cell-Mediated Immunity. *Immunity*. **52**, 606-619 (2020).

18. Y. Huang, L. Guo, J. Qiu, X. Chen, J. Hu-Li, U. Siebenlist, P. R. Williamson, J. F. Urban, W. E. Paul, IL-25-responsive, lineage-negative KLRG1 hi cells are multipotential "inflammatory" type 2 innate lymphoid cells. *Nat. Immunol.* **16**, 161–169 (2015).

19. H. J. McSorley, N. F. Blair, K. A. Smith, A. N. J. McKenzie, R. M. Maizels, Blockade of IL-33 release and suppression of type 2 innate lymphoid cell responses by helminth secreted products in airway allergy. *Mucosal Immunol.* **7**, 1068–78 (2014).

20. A. S. Mirchandani, A.-G. Besnard, E. Yip, C. Scott, C. C. Bain, V. Cerovic, R. J. Salmond, F. Y. Liew, Type 2 innate lymphoid cells drive CD4+ Th2 cell responses. *J. Immunol.* **192**, 2442–8 (2014).

21. C. J. Oliphant, Y. Y. Hwang, J. A. Walker, M. Salimi, S. H. Wong, J. M. Brewer, A. Englezakis, J. L. Barlow, E. Hams, S. T. Scanlon, G. S. Ogg, P. G. Fallon, A. N. J. McKenzie, MHCII-mediated dialog between group 2 innate lymphoid cells and CD4+ T cells potentiates type 2 immunity and promotes parasitic helminth expulsion. *Immunity*. **41**, 283–295 (2014).

22. M. J. Lecomte, C. Bertolus, J. Santamaria, A. L. Bauchet, M. Herbin, F. Saurini, H. Misawa, T. Maisonobe, P. F. Pradat, M. Nosten-Bertrand, J. Mallet, S. Berrard, Selective disruption of

acetylcholine synthesis in subsets of motor neurons: A new model of late-onset motor neuron disease. *Neurobiol. Dis.* **65**, 102–111 (2014).

23. S.-J. Chou, Z. Babot, A. Leingartner, M. Studer, Y. Nakagawa, D. D. M. O'Leary, Geniculocortical Input Drives Genetic Distinctions Between Primary and Higher-Order Visual Areas. *Science.* **340**, 1239–1242 (2013).

24. Y. Omata, M. Frech, T. Primbs, S. Lucas, D. Andreev, C. Scholtysek, K. Sarter, M. Kindermann, N. Yeremenko, D. L. Baeten, N. Andreas, T. Kamradt, A. Bozec, A. Ramming, G. Krönke, S. Wirtz, G. Schett, M. M. Zaiss, Group 2 Innate Lymphoid Cells Attenuate Inflammatory Arthritis and Protect from Bone Destruction in Mice. *Cell Rep.* **24**, 169–180 (2018).

25. J. V. Fahy, B. F. Dickey, Airway Mucus Function and Dysfunction. *N. Engl. J. Med.* **363**, 2233–2247 (2010).

26. A. E. Price, H.-E. Liang, B. M. Sullivan, R. L. Reinhardt, C. J. Eisley, D. J. Erle, R. M. Locksley, Systemically dispersed innate IL-13-expressing cells in type 2 immunity. *Proc. Natl. Acad. Sci.* **107**, 11489–11494 (2010).

27. L. Galle-Treger, Y. Suzuki, N. Patel, I. Sankaranarayanan, J. L. Aron, H. Maazi, L. Chen, O. Akbari, Nicotinic acetylcholine receptor agonist attenuates ILC2-dependent airway hyperreactivity. *Nat. Commun.* **7**, 1–13 (2016).

28. B. S. Kim, M. C. Siracusa, S. A. Saenz, M. Noti, L. A. Monticelli, G. F. Sonnenberg, M. R. Hepworth, A. S. Van Voorhees, M. R. Comeau, D. Artis, TSLP elicits IL-33-independent innate lymphoid cell responses to promote skin inflammation. *Sci. Transl. Med.* **5**, 170ra16 (2013).

29. H. Kim, Y. Chang, S. Subramanian, Innate lymphoid cells responding to IL-33 mediate airway-hyperreactivity independent of adaptive immunity. *J. Allergy Clin. Immunol.* **129**, 216–227 (2012).

30. B. Roediger, R. Kyle, S. S. Tay, A. J. Mitchell, H. A. Bolton, T. V. Guy, S. Y. Tan, E. Forbes-Blom, P. L. Tong, Y. Köller, E. Shklovskaya, M. Iwashima, K. D. McCoy, G. Le Gros, B. Fazekas De St Groth, W. Weninger, IL-2 is a critical regulator of group 2 innate lymphoid cell

function during pulmonary inflammation. *J. Allergy Clin. Immunol.* **136**, 1653-1663 (2015).

31. J. C. Nussbaum, S. J. Van Dyken, J. von Moltke, L. E. Cheng, A. Mohapatra, A. B. Molofsky, E. E. Thornton, M. F. Krummel, A. Chawla, H.-E. Liang, R. M. Locksley, Type 2 innate lymphoid cells control eosinophil homeostasis. *Nature*. **502**, 245–248 (2013).

32. J.-E. Turner, P. J. Morrison, C. Wilhelm, M. Wilson, H. Ahlfors, J.-C. Renauld, U. Panzer, H. Helmby, B. Stockinger, IL-9-mediated survival of type 2 innate lymphoid cells promotes damage control in helminth-induced lung inflammation. *J. Exp. Med.* **210**, 2951–65 (2013).

33. C. S. N. Klose, T. Mahlakõiv, J. B. Moeller, L. C. Rankin, A. L. Flamar, H. Kabata, L. A. Monticelli, S. Moriyama, G. G. Putzel, N. Rakhilin, X. Shen, E. Kostenis, G. M. König, T. Senda, D. Carpenter, D. L. Farber, D. Artis, The neuropeptide neuromedin U stimulates innate lymphoid cells and type 2 inflammation. *Nature*. **549**, 282–286 (2017).

34. O. Lockridge, Review of human butyrylcholinesterase structure, function, genetic variants, history of use in the clinic, and potential therapeutic uses. *Pharmacol. Ther.* **148**, 34–46 (2015).

35. H. Moriya, Y. Takagi, T. Nakanishi, M. Hayashi, T. Tani, I. Hirotsu, Affinity profiles of various muscarinic antagonists for cloned human muscarinic acetylcholine receptor (mAChR) subtypes and mAChRs in rat heart and submandibular gland. *Life Sci.* **64**, 2351–2358 (1999).

36. F. Dorje, J. Wess, G. Lambrecht, R. Tacke, E. Mutschler, M. R. Brann, Antagonist binding profiles of five cloned human muscarinic receptor subtypes. *J. Pharmacol. Exp. Ther.* **256**, 727–733 (1991).

37. R. Gosens, J. Zaagsma, H. Meurs, A. J. Halayko, Muscarinic receptor signaling in the pathophysiology of asthma and COPD. *Respir. Res.* **7**, 1–15 (2006).

38. I. S. T. Bos, R. Gosens, A. B. Zuidhof, D. Schaafsma, A. J. Halayko, H. Meurs, J. Zaagsma, Inhibition of allergen-induced airway remodelling by tiotropium and budesonide: A comparison. *Eur. Respir. J.* **30**, 653–661 (2007).

39. B. Bosnjak, C. Tilp, C. Tomsic, G. Dekan, M. P. Pieper, K. J. Erb, M. M. Epstein, Tiotropium bromide inhibits relapsing allergic asthma in BALB/c mice. *Pulm. Pharmacol. Ther.* **27**, 44–51 (2014).

40. S. Ohta, N. Oda, T. Yokoe, A. Tanaka, Y. Yamamoto, Y. Watanabe, K. Minoguchi, T.

Ohnishi, T. Hirose, H. Nagase, K. Ohta, M. Adachi, Effect of tiotropium bromide on airway inflammation and remodelling in a mouse model of asthma. *Clin. Exp. Allergy*. **40**, 1266–1275 (2010).

41. L. a. Monticelli, D. Artis, Innate lymphoid cells promote lung tissue homeostasis following acute influenza virus infection. *Nat. Immunol.* **12**, 1045–1054 (2011).

42. A. B. Molofsky, J. C. Nussbaum, H. E. Liang, S. J. V. Dyken, L. E. Cheng, A. Mohapatra, A. Chawla, R. M. Locksley, Innate lymphoid type 2 cells sustain visceral adipose tissue eosinophils and alternatively activated macrophages. *J. Exp. Med.* **210**, 535–549 (2013).

43. S. H. Wong, J. A. Walker, H. E. Jolin, L. F. Drynan, E. Hams, A. Camelo, J. L. Barlow, D. R. Neill, V. Panova, U. Koch, F. Radtke, C. S. Hardman, Y. Y. Hwang, P. G. Fallon, A. N. J. McKenzie, Transcription factor RORα is critical for nuocyte development. *Nat. Immunol.* **13**, 229–36 (2012).

44. T. Y. F. Halim, A. MacLaren, M. T. Romanish, M. J. Gold, K. M. McNagny, F. Takei, Retinoic-Acid-Receptor-Related Orphan Nuclear Receptor Alpha Is Required for Natural Helper Cell Development and Allergic Inflammation. *Immunity*. **37**, 463–474 (2012).

45. D. N. Cook, H. S. Kang, A. M. Jetten, Retinoic Acid-Related Orphan Receptors (RORs): Regulatory Functions in Immunity, Development, Circadian Rhythm, and Metabolism. *Nucl. Recept. Res.* **2**, 139–148 (2015).

46. R. M. Maizels, H. H. Smits, H. J. McSorley, Modulation of Host Immunity by Helminths: The Expanding Repertoire of Parasite Effector Molecules. *Immunity*. **49**, 801–818 (2018).

47. M. E. Selkirk, O. Lazari, J. B. Matthews, Functional genomics of nematode acetylcholinesterases. *Parasitology*. **131**, S3-18 (2005).

48. M. Camberis, G. Le Gros, J. Urban, Animal model of Nippostrongylus brasiliensis and Heligmosomoides polygyrus. *Curr. Protoc. Immunol.* 19, Unit 19.12 (2003).

49. W. G. C. Horsnell, M. G. Darby, J. C. Hoving, N. Nieuwenhuizen, H. J. McSorley, H. Ndlovu, S. Bobat, M. Kimberg, F. Kirstein, A. J. Cutler, B. DeWals, A. F. Cunningham, F. Brombacher, IL-4Rα-Associated Antigen Processing by B Cells Promotes Immunity in Nippostrongylus brasiliensis Infection. *PLoS Pathog.* **9**, 1–12 (2013).

Acknowledgments

We thank Mark Bennett for mass spectrometric determination of ACh, Henry McSorley for the kind gift of *Alternaria alternata* extract, Marc Le Bert for technical assistance with mouse genetics, and Jane Srivistava, Catherine Simpson and Nicolas Riteau for technical assistance with flow cytometry-assisted cell sorting.

Funding: We thank the Wellcome Trust and the BBSRC for supporting this work through a PhD studentship to LBR (097011) and a project grant to MES and DW (BB/R015856/1). This work was also supported by core funding from the Wellcome Trust (203135/Z/16/Z). RV was supported by a Medical Research Council PhD studentship (MR/J500379/1), and RB was initially supported by a scholarship from the Association Philippe Jabre (apj.org.ib). Royal Society International Exchange grant: IES\R1\180108, LeStudium - Marie Curie Fellowship, Centre National de la Recherche Scientifique (CNRS), and the European Regional Development Fund (FEDER N° 2016-00110366 and EX005756) supported work by JP, DS, CM, BR, VQ and WGCH. . NRF Competitive Support for Rated Researchers grant: 111815 supported work by MD, JP and WGCH. MJO and NP were supported by the Norwegian Research Council (Centre of Excellence grant 223255/F50, and 'Young Research Talent' 274760 to MJO).

Author contributions: Conception and design: LBR MES CS WGCH BR VQ KG DRW. Experimental: Cellular/immunological work: LBR CS RB MD CM DS RV WGCH; Histology: NP MJO JP; Parasitology: WGCH MES; Generation and genotyping of mice SB CM MES. Statistical analysis LBR RB MD MJO JP WGCH; Interpretation: LBR CS MD JP MJO NP WGCH MES. Drafting the manuscript: LBR WGCH MES.

Competing interests: The authors declared no competing interests.

Data and materials availability: *Ror*a^{Cre+}*Chat*^{LoxP} mice are available from Prof Bernhard Ryffel under a material agreement with INEM/CNRS-Orleans

Figure Legends

Figure 1. Pulmonary ILC2s acquire a cholinergic phenotype associated with an enhanced activation state during infection with *Nippostrongylus brasiliensis*. A) Proportion and total number of $CD45^+$ leukocytes expressing ChAT-eGFP in the lungs of naïve $ChAT^{BAC}$-eGFP mice or animals infected with *N. brasiliensis* (*Nb*) at day (D) 2,4,7, and 21 post infection (p.i.). **B)** Proportion of parental leukocyte populations expressing ChAT-eGFP in the lungs of naïve $ChAT^{BAC}$-eGFP mice or animals infected with *Nb* at D4 p.i. **C)** Representative flow cytometry plots of ChAT-eGFP expression by ILC2s ($CD45^+CD90^+$Lineage-$CD127^+ICOS^+ST2^+$) in wild type C57BL/6J mice infected with *Nb* (eGFP gating control), naïve $ChAT^{BAC}$-eGFP animals or infected $ChAT^{BAC}$-eGFP animals at D7 p.i. **D)** Dynamics of ChAT expression by ILC2s in the lungs and BAL throughout infection with *Nb*. **E)** Expression of *Chat* transcripts assayed by RT-qPCR in FACS-sorted $eGFP^+$ and $eGFP^-$ pulmonary ILC2s from *Nb*-infected $ChAT^{BAC}$-eGFP animals, normalised to 18s rRNA expression and relative to expression from ILC2s from naïve controls. **F)** Quantification of basal acetylcholine (ACh) release from FACS-sorted pulmonary ILC2s from C57BL6/J naïve and *Nb*-infected animals. **G)** Mean fluorescence intensity (MFI) of ST2 expressed by ChAT-eGFP negative and ChAT-$eGFP^+$ ILC2s in the lungs throughout infection with *Nb*. **H)** Geometric MFI (gMFI) of ICOS expressed by ChAT-$eGFP^-$ and ChAT-$eGFP^+$ ILC2s in the lungs throughout infection with *Nb*. Joined data points in (H-G) represent $ChAT^+$ and $ChAT^-$ ILC2 from individual mice. n = 3 to 5 mice/group. Data are representative of N = 3 and graphs present mean ± SEM. *p<0.05, **p<0.01, ***p< 0.001, ****p<0.0001, n.s. = non-significant (p>0.05).

Figure 2. ChAT-$eGFP^+$ ILC2s display a range of phenotypes which support positive association of ChAT expression by ILC2s with cellular activation state. A) Identification of population clusters (left) representing natural ILC2 (nILC2: IL17RB$^-$ST2$^+$Klrg1$^-$CD90^{hi}), inflammatory ILC2 (iILC2: IL17RB$^+$ST2^{lo}Klrg1$^+$CD90^{lo}) and nILC2/iILC2 with an activated-like phenotypic profile (nILC2a: IL17RB$^-$ST2$^+$Klrg1$^+$CD90$^+$, iILC2a: IL17RB$^+$ST2$^+$Klrg1$^+$CD90$^+$) within the lungs of *N. brasiliensis* (*Nb*)-infected ChAT-$eGFP^{BAC}$ mice at day 7 post infection (D7 p.i.). Clustering analysis was conducted using t-distributed stochastic neighbour embedding (t-SNE), with the parameter of ChAT-eGFP expression omitted, carried out on total lung ILC2s (identified as live, single cells,

790 $CD45^{+}Lineage^{neg}CD127^{+}ICOS^{+}CD90^{+}$ and expressing either or both ST2 and/or IL-17RB) with
791 indicated populations identified on the basis of various phenotypic markers and marker expression levels
792 as indicated by the heatmap plots shown (right). **B)** Heatmap plot showing locations of greatest ChAT-
793 eGFP expression amongst ILC2 clusters as defined through t-SNE in (A). **C)** Clustering analysis carried
794 out by t-distributed stochastic neighbour embedding (t-SNE) as in (A) but with the parameter of ChAT-
795 eGFP expression included (left) and heatmap plot of ChAT-eGFP expression to identify $ChAT^{+}$ cell
796 clusters, designated C1, C2 and C3 (right). **D)** Representative histogram overlays of indicated marker
797 expression for the indicated populations identified within a given biological samples. **E)** Contributions
798 of populations C1, C2, C3 to total ChAT-$eGFP^{+}$ ILC2 present in the lungs of ChAT-$eGFP^{BAC}$ mice at
799 D7 p.i, expressed as the contributing proportion of each population to the total. **F)** Representative
800 histogram overlays for the indicated marker expressions of total ChAT-$eGFP^{+}$ and ChAT-$eGFP^{neg}$
801 ILC2s (identified as live, single cells, $CD45^{+}Lineage^{neg}CD127^{+}ICOS^{+}CD90^{+}$ and expressing either or
802 both ST2 and/or IL-17RB) present in the lungs of naïve and infected ChAT-$eGFP^{BAC}$ mice at D7 p.i..
803 **G)** Mean fluorescence intensity (MFI) of ST2 expressed by total ILC2 and ChAT-eGFP negative and
804 ChAT-$eGFP^{+}$ ILC2s in the lungs of naïve and infected mice as in (F). **H)** As for (G) but for ICOS
805 geometric MFI (gMFI). Data are representative of observations and population comparisons made in n
806 = 3 male ChAT-$eGFP^{BAC}$ mice in both naïve and infected treatment groups. Data shown as mean ± SEM
807 and analyzed by Shapiro-Wilk normality testing followed by Welch's t-test , *$p<0.05$, **$p<0.01$. n.s. =
808 non-significant ($p>0.05$).
809
810 **Figure 3. Mesenteric lymph node ILC2s upregulate expression of ChAT following infection with**
811 ***Nippostrongylus brasiliensis*. A)** Representative flow cytometry gating indicating identification of total
812 ILC2s and ChAT-$eGFP^{+}$ and ChAT-$eGFP^{neg}$ ILC2s from the mesenteric lymph nodes (MLNs) of naïve
813 and infected ChAT-$eGFP^{BAC}$ mice at D7 p.i. *N. brasiliensis* -infected C57BL/6J control sampled
814 included to indicate ChAT-$eGFP^{+}$ gating control. **B)** Quantification of ChAT-eGFP+ ILC2s from naïve
815 and D7 p.i. ChAT-$eGFP^{BAC}$ mice expressed as a proportion of total ILC2s as shown in **(A)**. **C)**
816 Quantification of the number of total, ChAT-$eGFP^{+}$ and ChAT-$eGFP^{neg}$ ILC2s from MLNs of naïve and
817 D7 p.i. ChAT-$eGFP^{BAC}$ mice. **D)** Representative histogram overlays for the indicated marker

818 expressions of total ChAT-eGFP^{+} and ChAT-eGFP^{neg} MLN ILC2s **of** naïve and infected ChAT-
819 eGFP^{BAC} mice at D7 p.i.. **E)** Mean fluorescence intensity (MFI) of ST2 expressed by total ILC2 and
820 ChAT-eGFP negative and ChAT-eGFP^{+} ILC2s in the MLNs of naïve and infected mice as in (D). **F)** As
821 for (E) but for ICOS geometric MFI (gMFI)**. G)** Representative flow cytometry plot of ChAT-eGFP
822 expression by small intestinal lamina propria (siLP) ILC2s in naïve ChAT^{BAC}-eGFP animals. Gate
823 number represents proportion of ILC2 parental gate. Data are representative of observations and
824 population comparisons made in n = 3 male ChAT-eGFP^{BAC} mice in both naïve and infected treatment
825 groups, other than data shown in (G) which are representative of results in n = 2 mice. Data shown as
826 mean $\pm$ SEM and analyzed by Shapiro-Wilk normality testing followed by Welch's t-test , *p<0.05,
827 *p<0.01, ***p<0.001, ****p<0.0001.
828
829 **Figure 4. The cholinergic phenotype of pulmonary ILC2s is induced by IL-25 and IL-33 and is**
830 **augmented by IL-2. A)** Proportion of pulmonary ILC2s expressing ChAT-eGFP following sorting by
831 FACS and 24 hr culture with medium only (control), IL-33 or IL-7. **B)** Proportion of ILC2s in the lungs
832 of ChAT^{BAC}-eGFP mice, 24 h following intranasal dosing with PBS, IL-33, IL-25, or thymic stromal
833 lymphopoietin (TSLP). **C)** As for (B) but for mean fluorescence intensity (MFI) of eGFP expressed by
834 ILC2s. **D)** As for (A) but for the parental leukocyte populations indicated. **E)** Representative flow
835 cytometry plot of IL-17RB expression by lung ILC2s in naïve ChAT^{BAC}-eGFP animals. Gate number
836 represents proportion of ILC2 (CD45^{+}CD90^{+}Lineage^{-}CD127^{+}ICOS^{+} then ST2^{+} and/or IL-17RB^{+} live
837 single cells). **F)** Quantification of IL-17RB^{+} lung ILC2s as in (E). **G)** Proportion of ChAT-eGFP^{+} ILC2s
838 following *in vitro* culture of FACS purified total lung CD45^{+} cells for 24 h with the indicated
839 combinations of IL-33, IL-25 and IL-2. **H)** As for (G) but for eGFP MFI of ILC2s. n = 3-5 animals per
840 group. Data (A-D) and (G-H) are representative of N = 2 . Data (E-F) are representative of n = 3 mice
841 per treatment group. Graphs present mean $\pm$ SEM. Analysis carried out by Shapiro-Wilk test followed
842 by Welch's t-test. *p<0.05, **p<0.01, ***p< 0.001, n.s. = non-significant (p>0.05).
843
844 **Figure 5. RoRα-driven disruption of ChAT expression impairs pulmonary type 2 immunity and**
845 **expulsion of *Nippostrongylus brasiliensis* from the gut. A)** Recovery of worms from the lungs and

intestines of *Chat*^{LoxP} and *Rora*$^{Cre+}$*Chat*^{LoxP} mice at Day 2 (D2) and D6 post infection (p.i.) respectively, with *N. brasiliensis* (*Nb*) (N = 2-3) . **B)** Total number of eosinophils in the lungs of *Nb*-infected *Chat*^{LoxP} and *Rora*$^{Cre+}$*Chat*^{LoxP} mice at D6 p.i (N = 1). **C)** RT-qPCR analysis of *Il13* (left) and *Il5* (right) transcript expression in lung tissue of *Nb*-infected *Rora*$^{Cre+}$*Chat*^{LoxP} mice, represented as fold change against expression in infected *Chat*^{LoxP} lung samples. Each data point represents results from 1 animal. **D)** as for (C) but for analysis of *Muc5ac* and *Muc5b* expression. **E)** Representative lung sections from D6 *Nb*-infected *Chat*^{LoxP} and *Rora*$^{Cre+}$*Chat*^{LoxpP}mice (2 per genotype) showing Periodic Acid-Schiff' (PAS) and Hematoxylin and Eosin (H&E) staining (scale bar: 100 μm). **F)** Quantification of PAS stained lung sections (n = 5 mice per group, data representative of N = 2). Data show mean ± SEM and analyzed by Mann-Whitney U test, *p<0.05, **p<0.01, n.s. = non-significant (p>0.05).

Figure 6. Impaired immunity to *Nippostrongylus brasiliensis* in *Rora*$^{Cre+}$*Chat*^{loxP} mice is associated with defective intestinal epithelial effector responses. A) Representative intestinal sections from *N. brasiliensis* (*Nb*)-infected *Chat*^{LoxP} and *Rora*$^{Cre+}$*Chat*^{LoxpP}mice at D7 p.i. (2 per genotype) showing Periodic Acid-Schiff' (PAS) staining (scale bar: 50 μm) at 40x and 100x magnification. **B)** Quantification of PAS stained sections from (A). **C)** Representative immunofluorescence staining for doublecortin-like kinase 1 (Dclk1) expressing Tuft cells (green) with DAPI counterstain (blue) in jejunal sections of *Nb*-infected *Chat*^{LoxP} and *Rora*$^{Cre+}$*Chat*^{LoxpP}mice at D7 p.i. at 20x magnification (scale bar: 50 μm). **D)** Quantification of Dclk1^{+} Tuft cells in crypt (left), villus (center) and crypt+villus (right) regions of sections as in (C). **E)** Quantification of Dclk1^{+} Tuft cells as in (H), expressed as the ratio of cells in villus/ crypt regions per biological replicate sample. Data represent n= 5-6 mice per experimental group, N = 2. Data shown as mean ± SEM and analyzed by Mann-Whitney U test, *p<0.05, **p<0.01, ***p<0.001, n.s. = non-significant (p>0.05).

Figure 7. RoRα-driven disruption of ChAT expression in ILC2 limits ILC2 proliferation. A) Number of ILC2s in the lungs of naïve and *N. brasiliensis* (*Nb*)-infected *Chat*^{LoxP} and *Rora*$^{Cre+}$*Chat*^{LoxP} mice at D6 p.i. **B)** Total number of IL-13^{+} (left), IL-5^{+} (center) and IL-13^{+}IL-5^{+} ILC2s (right) in the lungs of naïve and *Nb*-infected (D6 p.i.) *Chat*^{LoxP} and *Rora*$^{Cre+}$*Chat*^{LoxP} mice. **C)** Representative flow

cytometry plots of Ki67 staining in lung ILC2s from naïve and *Nb*-infected *Chat*^{LoxP} and *Rora*$^{Cre+}$*Chat*^{LoxP} mice at D6 p.i. Gate numbers represent proportion of ILC2 parental gate. Positive gate set with fluorescence-minus-one control for Ki67. **D)** Summary data for proportion of Ki67^{+} lung ILC2s from naïve and infected *Chat*^{LoxP} and *Rora*$^{Cre+}$*Chat*^{LoxP} mice. **E)** as for (D) but for total number of Ki67^{+} ILC2. **F)** Representative histogram overlays for ICOS expression by lung ILC2s from naïve and *Nb*-infected *Chat*^{LoxP} and *Rora*$^{Cre+}$*Chat*^{LoxP} mice at D6.p.i. As all ILC2s are ICOS^{+}, ICOS^{neg} ILCs (CD45^{+}CD90^{+}Lineage^{-}CD127^{+}ICOS^{neg}) from Nb-infected *Chat*^{LoxP} mice are also shown as a biological negative control for ICOS expression. **G)** Summary data for ICOS mean fluorescence intensity (MFI) of lung ILC2s from naïve and infected *Chat*^{LoxP} and *Rora*$^{Cre+}$*Chat*^{LoxP} mice. **H)** Muscarinic acetylcholine receptor (mAChR) subtype expression analysis (*Chrm1*-5) conducted on cDNA from FACS sorted ChAT-eGFP^{+} and ChAT-eGFP^{neg} lung ILC2s of *Nb*-infected ChAT-eGFP^{BAC} mice, by endpoint PCR analysis, visualized by agarose gel electrophoresis. C57BL/6J brain tissue cDNA from was prepared and used as a positive control for AChR gene expressions. **I)** As for (H) but for analysis of nicotinic acetylcholine receptor (nAChR) alpha subunits (*Chrna1-5,7*) and beta subunits (*Chrnb1-4*) expressions. **J)** Representative flow cytometry plots and summary data **(K)** for Ki67 expression (represented as % of ILC2 parent) by FACS sorted C57BL/6J female lung ILC2s from *N. brasiliensis* -infected mice, cultured for 72 hours *in vitro* with recombinant IL-7 and IL-2 only (50 ng ml-^{1}) or in the presence of 10 μM of the muscarinic receptor antagonist 1,1-dimethyl-4-diphenylacetoxypiperidinium iodide (4-DAMP) or the nicotinic receptor antagonist mecamylamine hydrochloride (mecamylamine), or with an equivalent volume of reagent vehicles (dH20, DMSO) added to the culture medium (vehicle). **L)** Data from (K) expressed as vehicle control normalized values for each independent experimental run. Data A-G n = 5 mice/ group, N = 2. Data H-I are representative of cells pooled from n = 6 *Nb*-infected ChAT-eGFP^{BAC} mice, sorted as ChAT-eGFP^{+} and ChAT-eGFP^{neg} lung ILC2s at D11 p.i. Data J-L are representative of N = 4 with similar results (raw data shown in K, using cells pooled from n = 5 mice per experiment). Data show mean ± SEM and analyzed by Mann-Whitney U test, *p<0.05, **p<0.01, ***p< 0.001, ****p<0.0001, n.s. = non-significant (p>0.05).

Figures

Figure 1

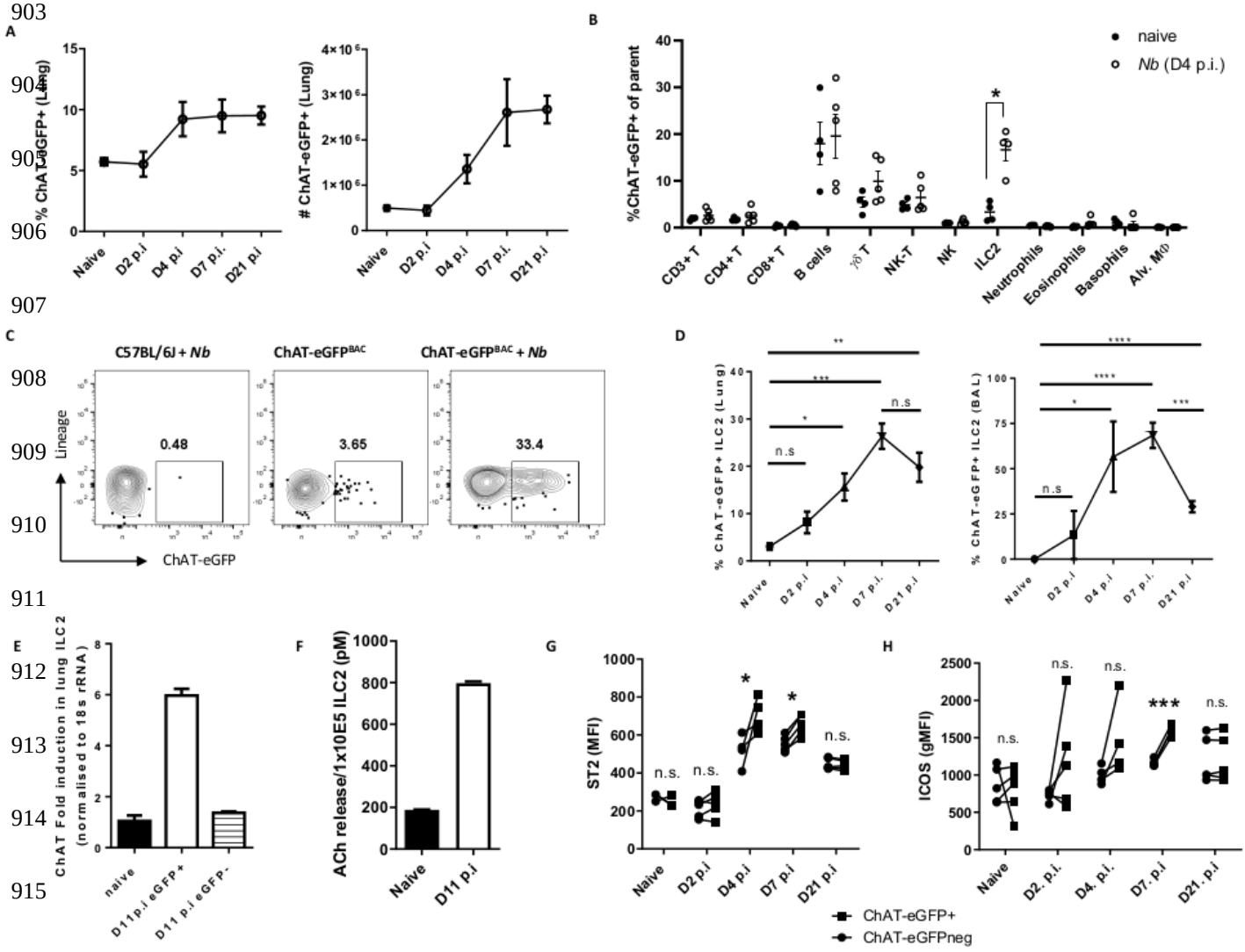

Figure 2

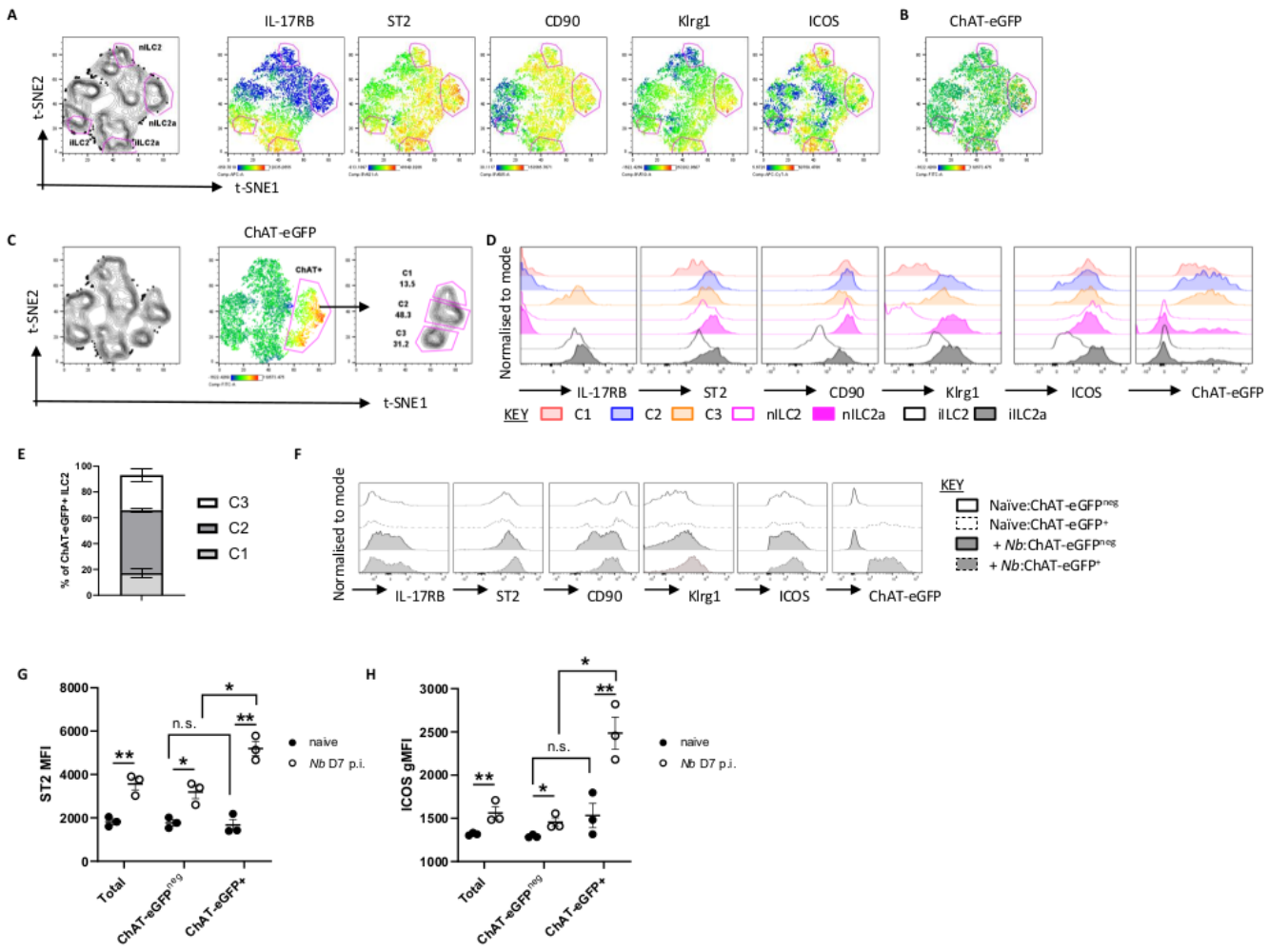
A
IL-17RB
ST2
CD90
Klrg1
ICOS
B
ChAT-eGFP
t-SNE2
t-SNE1
nILC2
nILC2a
iILC2
iILC2a
C
ChAT-eGFP
ChAT+
C1
13.5
C2
48.3
C3
31.2
D
Normalised to mode
IL-17RB
ST2
CD90
Klrg1
ICOS
ChAT-eGFP
KEY
C1
C2
C3
nILC2
nILC2a
iILC2
iILC2a
E
% of ChAT-eGFP+ ILC2
C3
C2
C1
F
Normalised to mode
KEY
Naïve:ChAT-eGFPneg
Naïve:ChAT-eGFP+
+ Nb:ChAT-eGFPneg
+ Nb:ChAT-eGFP+
G
ST2 MFI
naive
Nb D7 p.i.
n.s.
Total
ChAT-eGFPneg
ChAT-eGFP+
H
ICOS gMFI
naive
Nb D7 p.i.
n.s.
Total
ChAT-eGFPneg
ChAT-eGFP+

Figure 3

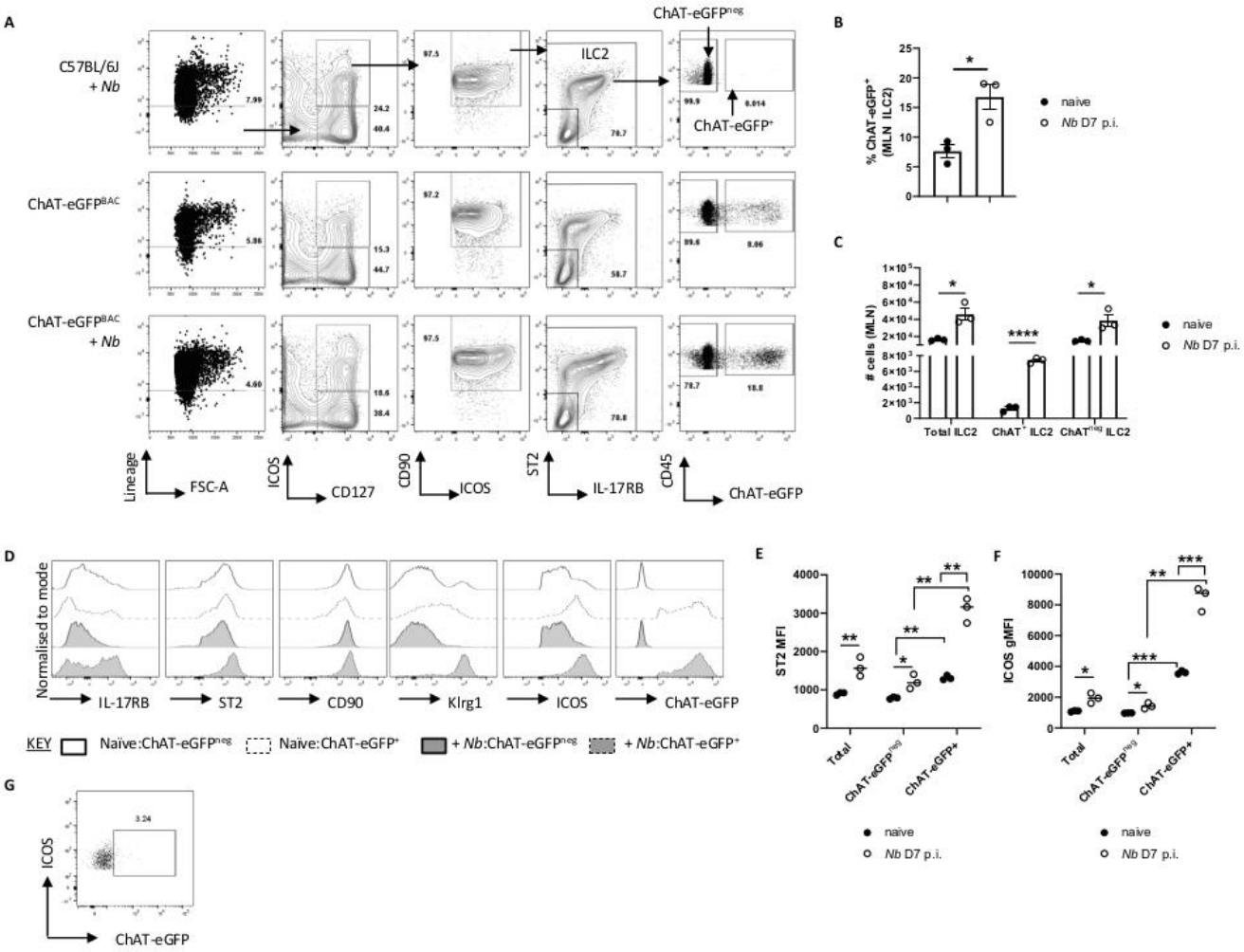
A
C57BL/6J + Nb
ChAT-eGFPBAC
ChAT-eGFPBAC + Nb
ILC2
ChAT-eGFPneg
ChAT-eGFP+
Lineage
FSC-A
ICOS
CD127
CD90
ICOS
ST2
IL-17RB
CD45
ChAT-eGFP
B
% ChAT-eGFP+ (MLN ILC2)
naive
Nb D7 p.i.
C
cells (MLN)
Total ILC2
ChAT+ ILC2
ChATneg ILC2
D
Normalised to mode
IL-17RB
ST2
CD90
Klrg1
ICOS
ChAT-eGFP
KEY
Naïve:ChAT-eGFPneg
Naïve:ChAT-eGFP+
+ Nb:ChAT-eGFPneg
+ Nb:ChAT-eGFP+
E
ST2 MFI
Total
ChAT-eGFPneg
ChAT-eGFP+
F
ICOS gMFI
G
ICOS
ChAT-eGFP

Figure 4

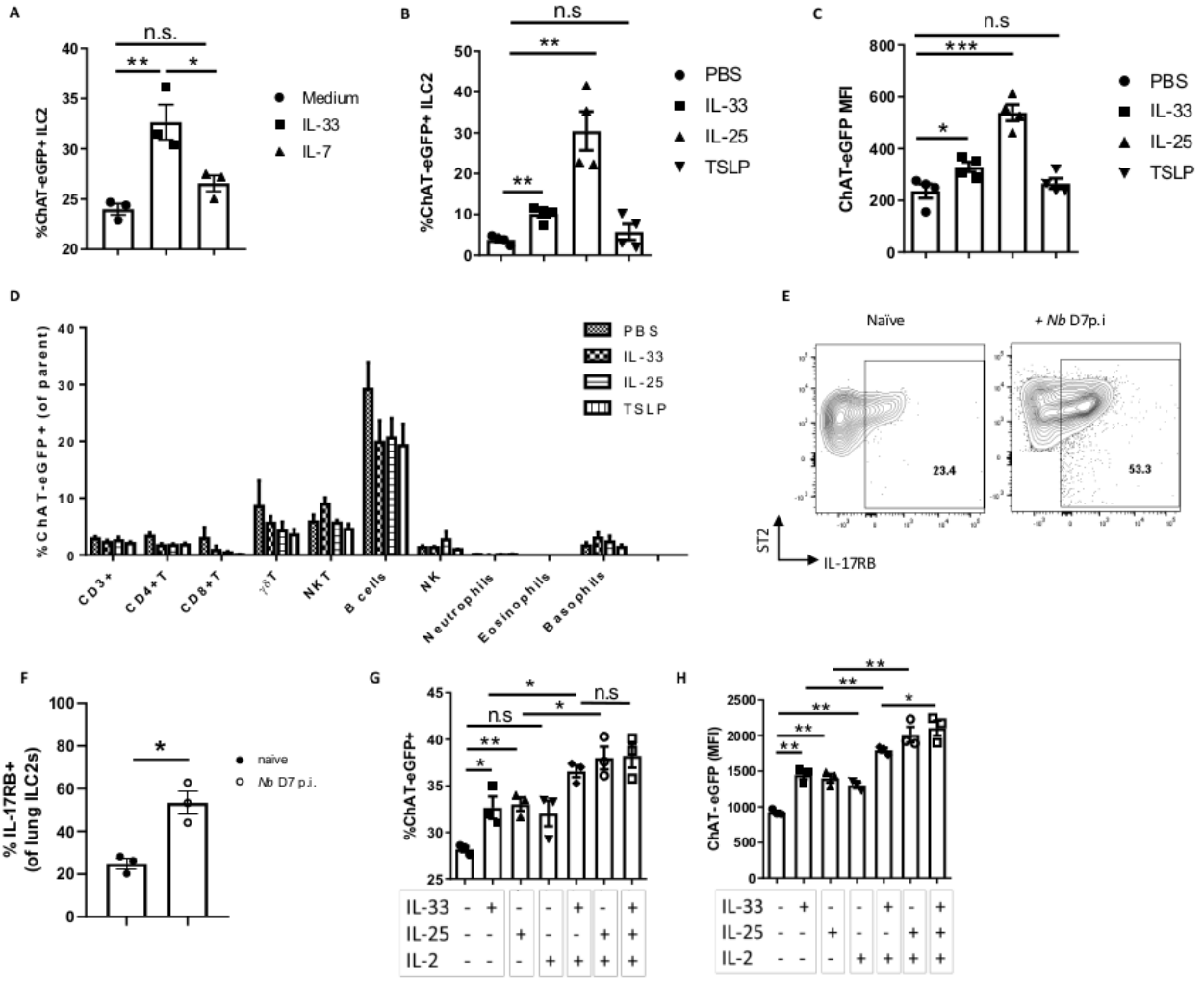
A
n.s.
%ChAT-eGFP+ ILC2
Medium
IL-33
IL-7
B
n.s
%ChAT-eGFP+ ILC2
PBS
IL-33
IL-25
TSLP
C
n.s
ChAT-eGFP MFI
PBS
IL-33
IL-25
TSLP
D
% ChAT-eGFP+ (of parent)
PBS
IL-33
IL-25
TSLP
CD3+
CD4+T
CD8+T
γδT
NKT
B cells
NK
Neutrophils
Eosinophils
Basophils
E
Naïve
+ Nb D7p.i
23.4
53.3
ST2
IL-17RB
F
% IL-17RB+ (of lung ILC2s)
naïve
Nb D7 p.i.
G
%ChAT-eGFP+
IL-33
IL-25
IL-2
H
ChAT-eGFP (MFI)
IL-33
IL-25
IL-2

Figure 5

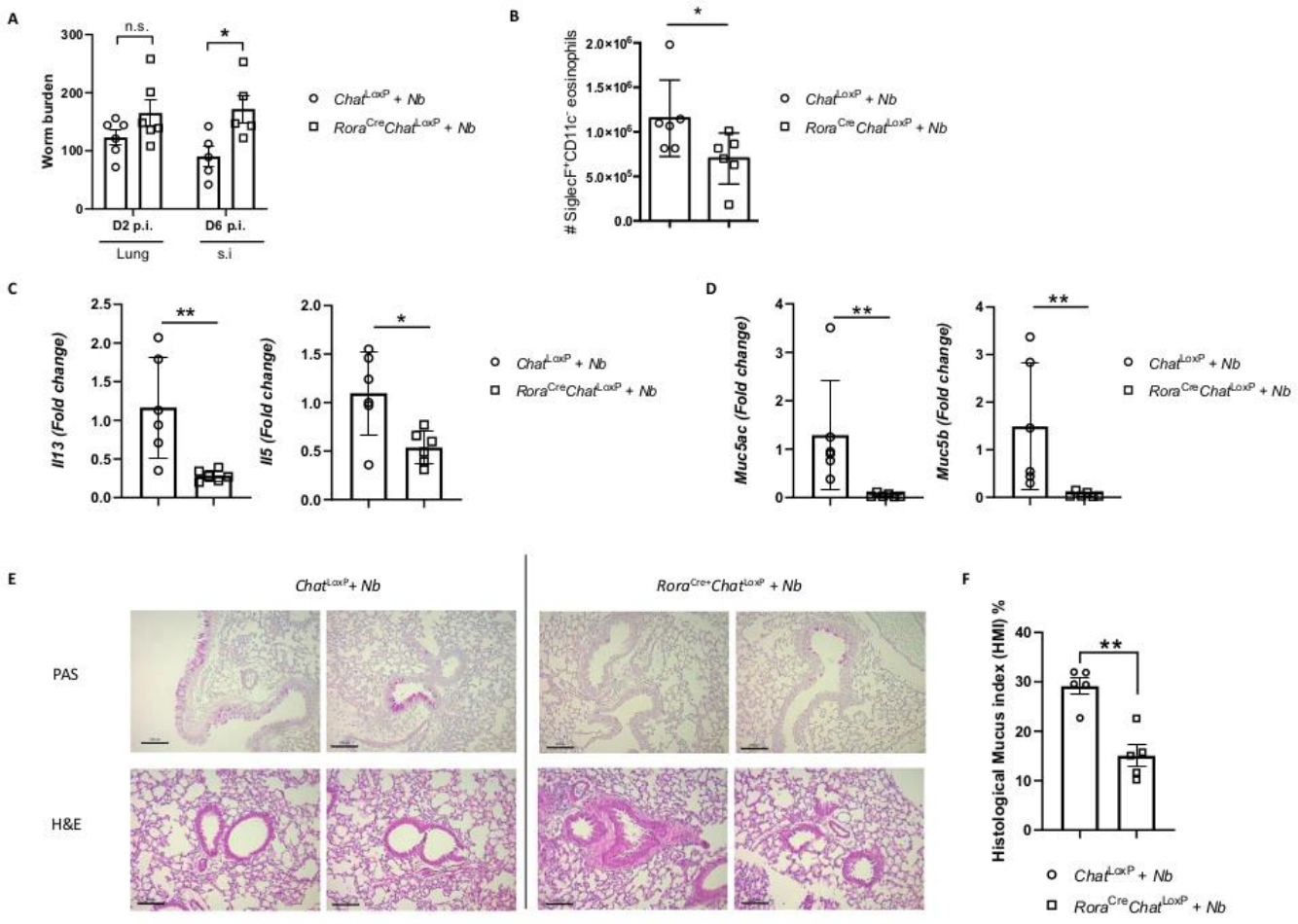
A
n.s.
*
Worm burden
300
200
100
0
D2 p.i.
D6 p.i.
Lung
s.i
Chat^LoxP + Nb
Rora^Cre Chat^LoxP + Nb
B
*
SiglecF+CD11c- eosinophils
2.0×10^6
1.5×10^6
1.0×10^6
5.0×10^5
0.0
Chat^LoxP + Nb
Rora^Cre Chat^LoxP + Nb
C
**
Il13 (Fold change)
2.5
2.0
1.5
1.0
0.5
0.0
*
Il5 (Fold change)
2.0
1.5
1.0
0.5
0.0
Chat^LoxP + Nb
Rora^Cre Chat^LoxP + Nb
D
**
Muc5ac (Fold change)
4
3
2
1
0
**
Muc5b (Fold change)
4
3
2
1
0
Chat^LoxP + Nb
Rora^Cre Chat^LoxP + Nb
E
Chat^LoxP + Nb
Rora^Cre Chat^LoxP + Nb
PAS
H&E
F
**
Histological Mucus index (HMI) %
40
30
20
10
0
Chat^LoxP + Nb
Rora^Cre Chat^LoxP + Nb

Figure 6

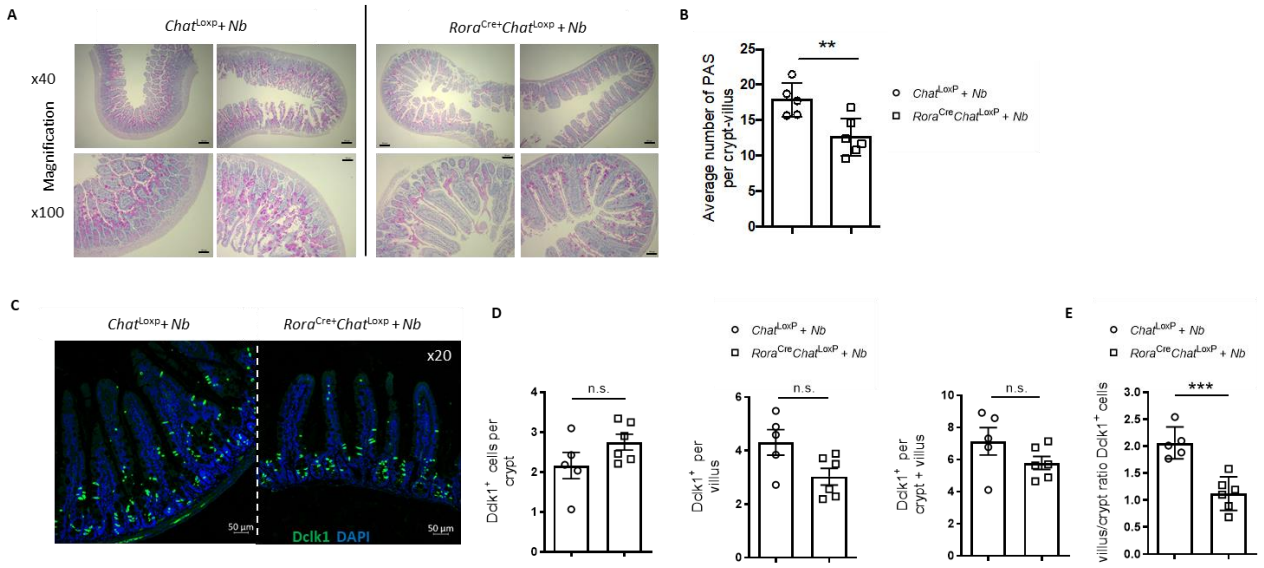
A
Chat^Loxp + Nb
Rora^Cre+Chat^Loxp + Nb
x40
Magnification
x100
B
Average number of PAS per crypt-villus
**
Chat^LoxP + Nb
Rora^CreChat^LoxP + Nb
C
Chat^Loxp + Nb
Rora^Cre+Chat^Loxp + Nb
x20
50 µm
Dclk1 DAPI
D
Dclk1+ cells per crypt
n.s.
Dclk1+ per villus
n.s.
Dclk1+ per crypt + villus
n.s.
E
villus/crypt ratio Dclk1+ cells
***

Figure 7

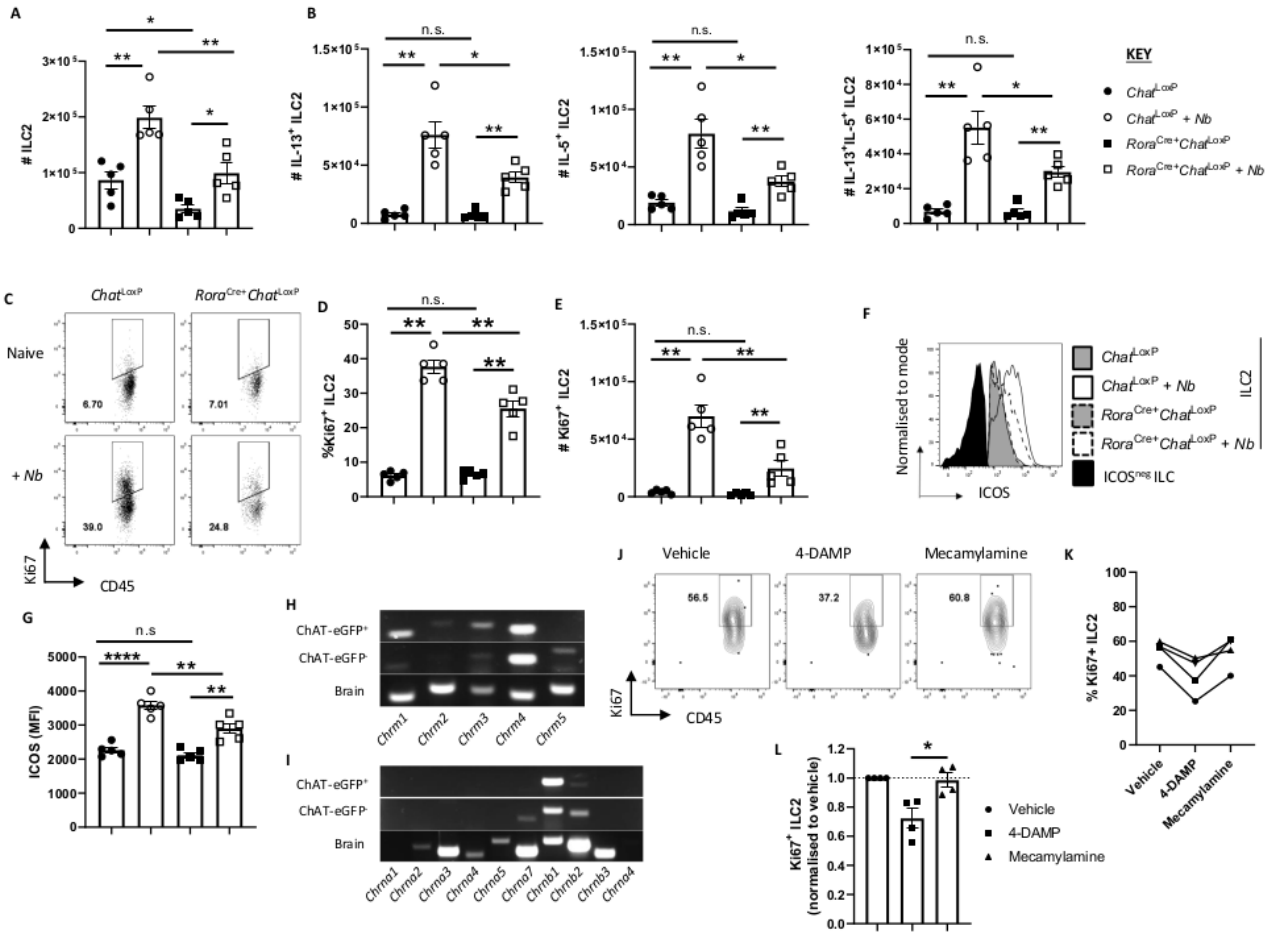
A
ILC2
B
IL-13+ ILC2
IL-5+ ILC2
IL-13+IL-5+ ILC2
n.s.
KEY
ChatLoxP
ChatLoxP + Nb
RoraCre+ChatLoxP
RoraCre+ChatLoxP + Nb
C
ChatLoxP
RoraCre+ChatLoxP
Naive
+ Nb
6.70
7.01
39.0
24.8
Ki67
CD45
D
%Ki67+ ILC2
E
Ki67+ ILC2
F
Normalised to mode
ICOS
ILC2
ICOSneg ILC
G
ICOS (MFI)
n.s
H
ChAT-eGFP+
ChAT-eGFP-
Brain
Chrm1
Chrm2
Chrm3
Chrm4
Chrm5
I
Chrna1
Chrna2
Chrna3
Chrna4
Chrna5
Chrna7
Chrnb1
Chrnb2
Chrnb3
Chrnb4
J
Vehicle
4-DAMP
Mecamylamine
56.5
37.2
60.8
K
% Ki67+ ILC2
L
Ki67+ ILC2 (normalised to vehicle)

Supplementary Materials

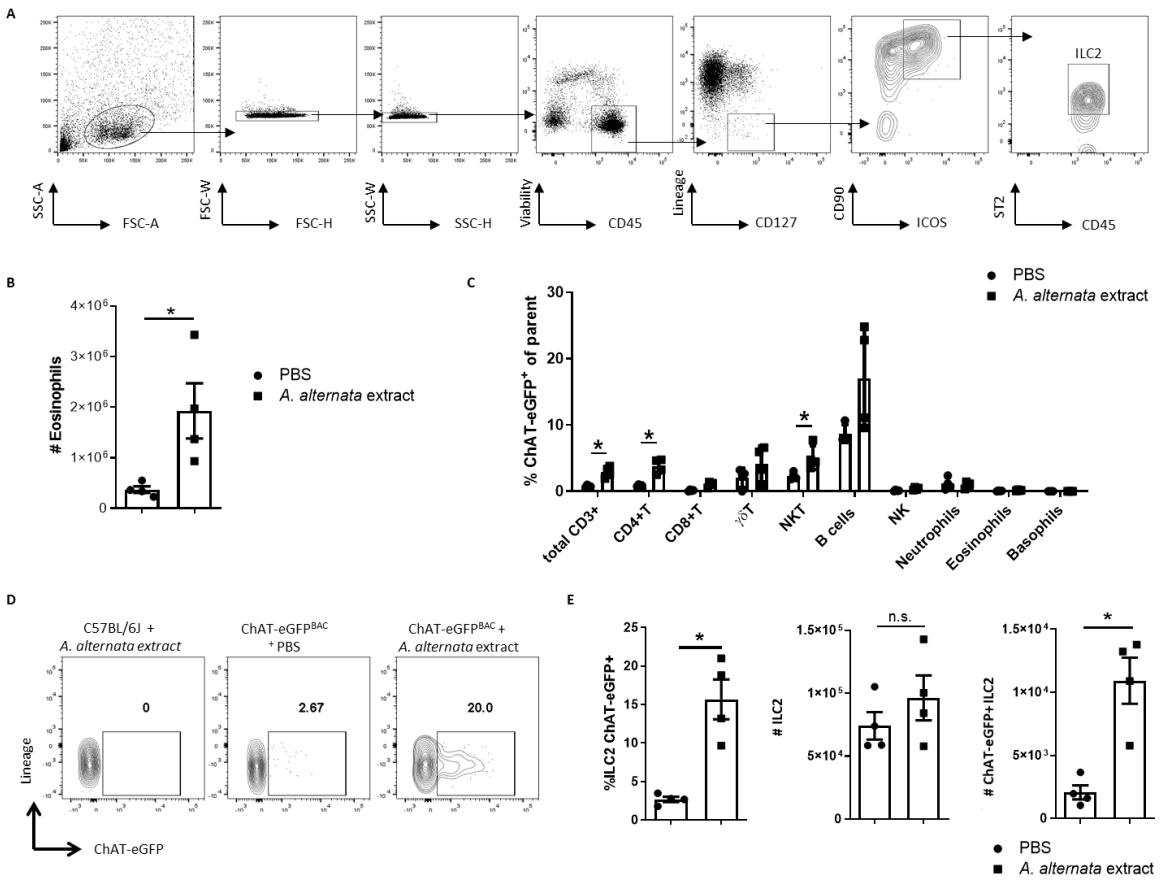

Figure S1. Pulmonary ILC2s acquire a cholinergic phenotype following exposure to *Alternaria alternata*. A) Representative gating strategy for identification of ILC2s by flow cytometry, as used in this study, unless otherwise stated. Tissue shown here is mouse lung. **B)** Intranasal administration of *Alternaria alternata* extract stimulates pulmonary eosinophilia. **C)**Proportion of parental cell populations expressing ChAT-eGFP in the lungs of ChAT^{BAC}-eGFP mice 24 hrs following intranasal dosing with PBS (vehicle control) or *A. alternata* extract. **D)** Representative flow cytometry plots of ChAT-eGFP expression by ILC2s in lungs of wild type C57BL/6J mice exposed to *A. alternata* extract (eGFP gating control), or ChAT^{BAC}-eGFP mice dosed with PBS or *A. alternata* allergenic extract. **E)** ILC2 responses in the lungs of ChAT^{BAC}-eGFP mice 24 hrs following intranasal dosing with PBS or *A. alternata* extract including (from left to right): proportion (%) of ChAT-eGFP+ ILC2s, total number (#) of ILC2s in the lung, and total number of ChAT-eGFP+ ILC2s. n = 4 mice/group. Data are representative of N=2 and represent mean ± SEM. *p<0.05, n.s. = non-significant (p>0.05).

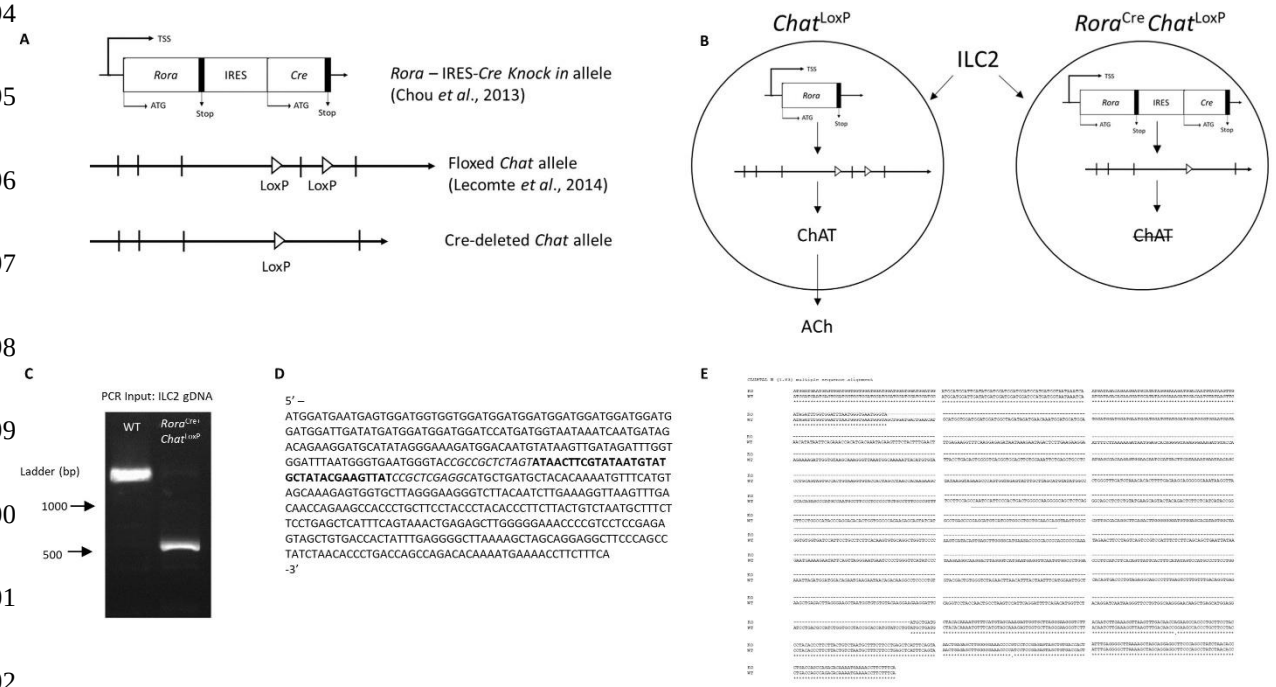

Figure S2. Generation of *Rora*$^{Cre+}$*Chat*^{loxP} and validation of *Chat* deletion in lung ILC2s. A) Schematic of the allele modifications undertaken to generate *Rora*$^{Cre+}$ (*Rora*-IRES-Cre) and *Chat*^{LoxP} mouse strains, based on the indicated publications. **B)** Schematic depicting inhibition of ChAT-mediated ACh synthesis by *Rora*$^{Cre+}$*Chat*^{LoxP} ILC2s. **C)** PCR products for amplification of *Chat* across the deleted exon. **D)** Sequence of PCR product shown in (C) for *Rora*$^{Cre+}$*Chat*^{LoxP} ILC2. The remaining LoxP sequence (ATAACTTCGTATAATGTATGCTATACGAAGTTAT) is shown in **Bold.** Sequence in *Italics* does not correspond to WT *Chat* sequence and is derived from the cassette used to place the Loxp sites into the *Chat* allele. **E)** Alignment of WT *Chat* genomic transcript and the sequence returned from ILC2s of *Rora*$^{Cre+}$*Chat*^{LoxP} mice after removal of LoxP and insertion cassette (see C). Position of coding exon 5 of WT murine *Chat* is underlined.

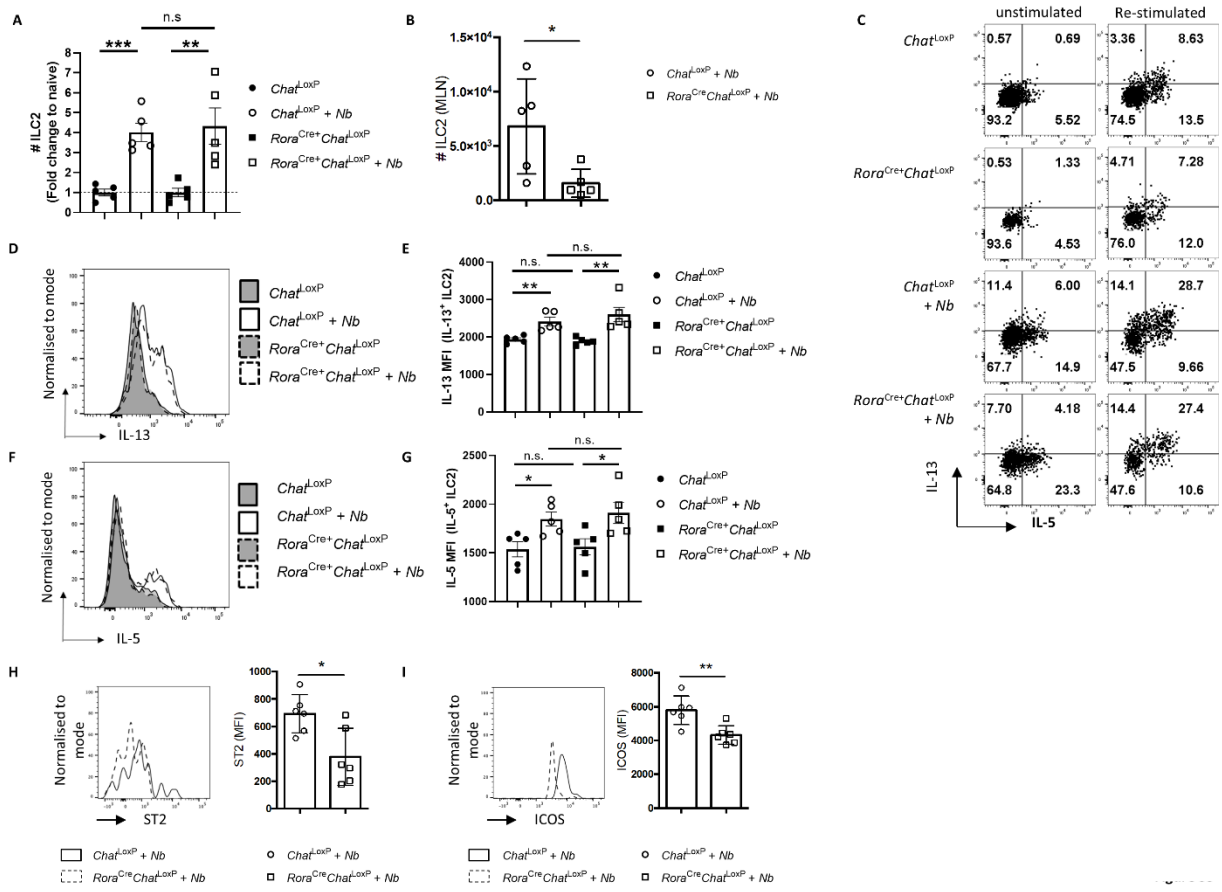

Figure S3. Pulmonary ILC2 cytokine measurements and assessment of numbers and activation markers of mesenteric lymph node ILC2s in *Chat*^{LoxP} and *Rora*$^{Cre+}$*Chat*^{LoxP} mice. A) Number of ILC2s in naïve and *N. brasiliensis* (*Nb*)-infected *Rora*$^{Cre+}$*Chat*^{LoxP} and *Chat*^{LoxP} mice expressed as the fold change from the average number of ILC2s in naïve mice of each genotype (normalized to a value of 1)**. B)** Number of ILC2s from mesenteric lymph nodes (MLN) of *Rora*$^{Cre+}$*Chat*^{LoxP} and *Chat*^{LoxP} mice infected with *Nb*. **C)** Representative flow cytometry plots for intracellular staining of lung ILC2 for IL-13 and IL-5 in unstimulated (Monensin only) and re-stimulated (PMA/Ionomycin+ Monensin) culture conditions. Quadrants were set using fluorescence minus one controls for IL-13 and IL-5. Quadrant numbers represent the proportion of the ILC2 parental population. **D)** Representative histogram overlays of IL-13 intracellular staining of lung ILC2 from re-stimulated lung samples and **(E)** summary of IL-13 mean fluorescence intensity (MFI) analysis of those samples. **F)** and **(G)** as for (D) and (E) respectively, but for intracellular staining of IL-5. **H)** Representative histogram overlays for ST2 expression by MLN ILC2s from infected *Chat*^{LoxP} and *Rora*$^{Cre+}$*Chat*^{LoxP} mice (left) and summary data for ST2 mean fluorescence intensity (MFI) of MLN ILC2s (right). **I)** As for (H) but for ICOS expression by MLN

ILC2s. Timepoints of infection were D6 p.i. in (A), (C-G) (n = 5 mice per group, N = 2) and D7 p.i. in (B), (H-I) (n = 6 mice per group, N=1). Timepoints Data represent mean ± SEM and analysed by Mann Whitney U test. *p<0.05,n.s. = non-significant (p>0.05).

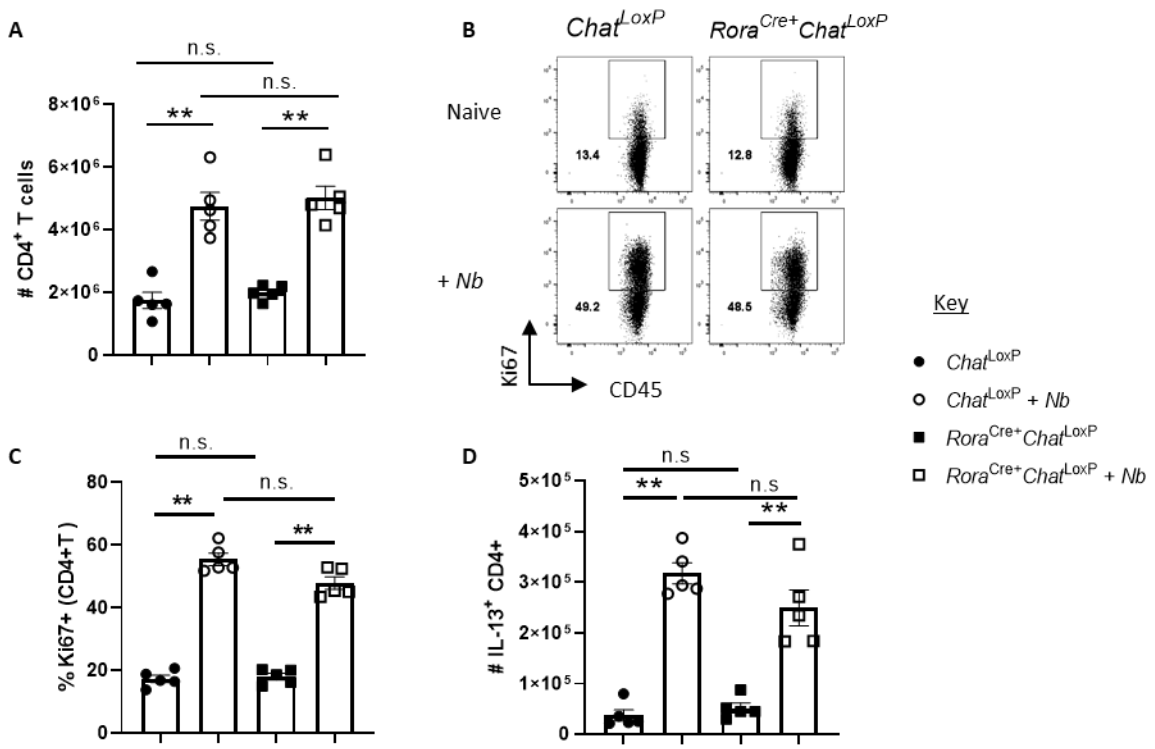

Figure S4. Pulmonary CD4$^+$ T cell numbers and capacity for Th$_2$ cytokine expression remains intact in *Rora*$^{Cre+}$*Chat*^{loxp} mice. A) Total number of CD4$^+$ T cells in the lungs of naïve and infected *Chat*^{LoxP} and *Rora*$^{Cre+}$*Chat*^{LoxP} mice. **B)** Representative flow cytometry plots of Ki67 staining in lung CD4$^+$ T cells from naïve and infected *Chat*^{LoxP} and *Rora*$^{Cre+}$*Chat*^{LoxP} mice. Gate numbers represent proportion of ILC2 parental gate. Positive gate set with fluorescence minus one control for Ki67. **C)** Proportion of lung CD4$^+$ T cells from naïve and *N. brasiliensis* (*Nb*)-infected *Chat*^{LoxP} and *Rora*$^{Cre+}$*Chat*^{LoxP} mice expressing Ki67. **D)** Number of IL-13$^+$ CD4$^+$ T cells in the lungs of naïve and infected *Chat*^{LoxP} and *Rora*$^{Cre+}$*Chat*^{LoxP} mice. n = 5 mice per group, N = 2. Timepoints of infection were D6 p.i. Data represent mean ± SEM and analysed by Mann Whitney U test. *p<0.05, **p<0.01, n.s. = non-significant (p>0.05).

Dated 2015

(1) Partner XY

(2) INEM - UMR7355, MOLECULAR IMMUNOLOGY, UNIVERSITY AND CNRS

Materials Transfer Agreement

MATERIALS TRANSFER AGREEMENT

THIS AGREEMENT is made on

BETWEEN

1. The University XY

2. INEM - UMR7355, Molecular Immunology, University and CNRS, 3b rue de la Ferollerie F-45071 Orleans - Cedex 2, France ("the Recipient Organisation")

BACKGROUND

The parties have agreed that the University will provide the Recipient Organisation with the biological materials as described below and the related Confidential Information as

defined below, which is the confidential and proprietary property of the University, upon the terms and conditions set out in this Agreement.

OPERATIVE PROVISIONS

1. INTERPRETATION

1.1 In this Agreement the following expressions have the following meanings unless inconsistent with the context:

"Confidential Information"	any and all knowledge, know-how, information, and/or techniques of a confidential or proprietary nature disclosed by the University to the Recipient Organisation relating to the Materials including, without limitation, all products, inventions, biological material, systems of production, research, data, specifications, software programs and samples, designs, photographs, drawings, plans, prototypes, models, documents, recordings, instructions, formulae, methodologies, processes, manuals, papers or other materials of any nature whatsoever, whether written or otherwise, relating to same
"Intellectual Property"	all intellectual and industrial property rights, including without limitation, patents, rights in know-how, trade marks, registered designs, models, unregistered design rights, unregistered trade marks and copyright (whether in drawings, plans, specifications, designs and computer software or otherwise), database rights, topography rights, any rights in any invention, discovery or process, and applications for and rights to apply for any of the foregoing, in each case in the United Kingdom and all countries in the world
"Materials"	*Rora*^{Cre}*Chat*^{LoxP} *mice*, supplied by the University to the Recipient Organisation and all unmodified progeny generated from the materials supplied and that part of all derivatives and the derivatives progeny which contains any of the materials supplied or its progeny
"Modifications"	substances created by the Recipient Organisation which contain or incorporate the Materials
"Purpose"	has the meaning set out in **clause 4.1.1**
"Recipient Scientist"	the principal scientist employed by the Recipient Organisation whose name is specified in the **Appendix**

1.2 All references to the Materials shall be taken to include any and all information and Intellectual Property to which the Recipient Organisation may be given access to by the University relating to or in connection with the Materials, including without limitation, data, formulae, processes, designs, photographs, drawings, specifications, software programs and samples and any other such material, in each case, however disclosed.

2. OWNERSHIP

2.1 All Intellectual Property in the Materials and the physical embodiment of the Materials themselves will remain the property of the University.

2.2 All rights (including all Intellectual Property) relating to the Materials and all Modifications shall remain the property of or rest in the University.

3. DELIVERY OF MATERIALS

3.1 The University shall send the Materials to the Recipient Organisation.

3.2 The University shall provide the Recipient Organisation with a copy of any protocols which the University may have concerning the handling, storage and safety of the Materials.

3.3 Should any government permit or licence be required for the transfer of the Materials to the Recipient Organisation, the Recipient Organisation shall obtain such permit or licence at its entire cost and expense and shall supply the same to the University prior to the despatch of the Materials.

4. USE OF THE MATERIALS

4.1 The Recipient Organisation agrees that:

4.1.1 the Materials are provided to the Recipient Organisation on a non-exclusive basis only for the purposes of research use only in laboratory animals or *in vitro* experiments *(**"the Purpose"**) and not for administration to human subjects, for clinical or diagnostic purposes involving human subjects, or for commercial purposes;*

4.1.2 the Materials are to be used only at the Recipient Organisation's premises and only in the Recipient Scientist's laboratory at those premises;

4.1.3 the Materials will be handled and stored in accordance with any reasonable protocols provided to the Recipient Organisation in accordance with **clause 3.2***;*

4.1.4 the Materials will be used only by individuals working within the Recipient Organisation, and will not be transferred, distributed, or released to any other person, firm or institution; *and*

4.1.5 the Materials are not made available to anyone other than employees of the Recipient Organisation engaged in carrying out the Purpose and shall not be further distributed to others without the University's prior written consent. The Recipient Organisation shall refer any request for the Materials to the University.

4.2 The Recipient Organisation agrees to use the Materials in compliance with all applicable statutes and regulations and under suitable containment conditions.

5. CONFIDENTIALITY

5.1 In consideration of the University disclosing the Materials to the Recipient Organisation, the Recipient Organisation agrees to keep all Confidential Information associated with the Materials which is disclosed by the University to the Recipient Organisation secret and confidential and not to disclose or transfer the same or permit the same to be disclosed or transferred to any third party for any reason whatsoever.

5.2 The Recipient Organisation will keep any confidential materials passed to the Recipient Organisation by the University at the premises of the Recipient Organisation in a secure environment, protected against theft, damage, loss, misuse or unauthorised access.

6. RESULTS & COMMERCIALISATION

6.1 The Recipient Organisation will inform the University in confidence of research results relating to or created using the Materials by written communication or by providing the University with a manuscript describing the results of such research at the time the manuscript is submitted for publication. If publication results from research using the Materials, acknowledgement of and/or credit will be given to the University as the source of the Materials.

6.2 If the Recipient Organisation or any of its employees, including the Recipient Scientist, wishes to include in a publication any information which has been provided by the University and which is "confidential" the Recipient Organisation shall not publish without written permission from the University and shall provide the University with a copy of the proposed text before publication takes place.

6.3 The Recipient Organisation shall have no right to use or permit the use of any products or processes containing, using or directly derived from the Materials for profit making or commercial purposes (**"Commercial Use"**). If the Recipient Organisation wishes to make Commercial Use of the Materials or any product directly derived from the Materials it shall request a licence from the University. The University shall have no obligation to grant any such licence to the Recipient Organisation.

6.4 Nothing in this Agreement, including any Intellectual Property protection being sought by the Recipient Organisation on any new use made of the Materials, shall prevent the University from being able to distribute the Materials to other commercial or non-commercial entities.

7. CONSIDERATION

7.1 The Materials are provided at no cost.

8. TERM AND TERMINATION

8.1 Unless terminated in accordance with **clause 8.2**, this Agreement shall take effect from the date set out at the beginning of this Agreement and shall remain in full force and effect for a period of 10 years.

8.2 The University may terminate this Agreement if the Recipient Organisation is in material breach of any of its terms and, where the breach is capable of remedy, the Recipient Organisation has failed to remedy the same within one month of service of a written notice from the University specifying the breach and requiring it to be remedied.

8.3 Notwithstanding any early termination of this Agreement, the obligations on the Recipient Organisation created in this Agreement shall survive and continue to be binding upon the Recipient Organisation, its successors and assigns for 3 years from the date of termination or expiry of this Agreement.

8.4 Upon the termination or expiry of this Agreement, the Recipient Organisation shall cease using the Confidential Information and the Materials in any manner whatsoever and, upon written request by the University, the Recipient Organisation shall deliver up to the University or destroy all of the Confidential Information and Materials in or under the Recipient Organisation's possession or control.

9. LIABILITY

9.1 All characteristics of the Materials are not fully understood and their use may involve risks or dangers that are not known or fully appreciated. The Materials are being provided on an "as is" basis, without warranty of any sort, express or implied and the University will not be liable for any use made of the Materials or any claim that the Materials infringe the intellectual property rights of third parties.

9.2 So far as is permitted by law, the Recipient Organisation assumes all liability for damages which may arise from its receipt, use, storage or disposal of the Materials and it will hold the University and its employees harmless from any loss, claim, damage or liability, of any kind which may arise from or in connection with this Agreement or the use, handling or storage of the Materials. In no event shall the University be liable for any use by the Recipient Organisation of the Materials or

any loss, claim, damage or liability, of any kind which may arise from or in connection with this Agreement or the use, handling or storage of the Materials.

10. GENERAL

10.1 The Recipient Organisation shall not assign, transfer, charge or otherwise dispose of any or all of the rights, duties or obligations granted to it under this Agreement without the prior written consent of the University.

10.2 This Agreement may be executed in one or more counterparts each of which shall for all purposes be deemed to be an original and all of which shall constitute one and the same instrument. Each party agrees that executed counterparts may be exchanged by email as scanned pdf copies.

10.3 This Agreement and any non-contractual obligations arising out of or in connection with it shall be governed by and construed in all respects in accordance with the laws of England and the parties hereby submit to the non-exclusive jurisdiction of the English Courts.

On behalf of The University XY

Name:

Signature:

Position:

Date:

On behalf of INEM - UMR7355, Molecular Immunology, University and CNRS

Name:

Signature:

Position:

Date:

APPENDIX 1

	Recipient Organisation's Scientist
Name	**Bernhard Ryffel**
Title	**MD, PhD**
Full address	**INEM - UMR7355, Molecular Immunology, University and CNRS, 3b rue de la Ferollerie F-45071 Orleans - Cedex 2, France**